Referee #1

Alroe et al. present a set of aerosol and meteorological observations obtained during a three-week test cruise of the RV Investigator between Hobart, Australia and the marginal ice zone of Antarctica along longitude 146°. Measurements made during the cruise include aerosol size distributions between 4 and 673 nm, size distributions of ultrafine aerosol (2-42 nm) using a Neutral Cluster and Air Ion Spectrometer (NAIS) instrument, cloud condensation nuclei (CCN) concentration measurements at 0.5% supersaturation using a CCN counter, aerosol chemical composition measurements using an Aerosol Chemical Speciation Monitor (ACSM), aerosol hygroscopicity and volatility measurements using a Volatility and Hygroscopicity Tandem Differential Mobility Analyser (VH-TDMA), measurements of black carbon mass using a Multi-Angle Absorption Photometer (MAAP) and radon concentrations using a dual-flow-loop two-filter radon detector.
Using this extensive set of observations the authors draw several conclusions:
1. Although Aitken mode number fraction was around 75% on a number of occasions their relatively small median diameter (∼ 30 nm) meant that the presence of increased numbers of Aitken mode particles correlated poorly with measured CCN concentrations. This suggests that nss-SO 4 new particle formation in the region may have little influence on local cloud droplet number concentrations and that further cloud processing or nss-SO 4 condensation is required to grow them to cloud-active diameters.
2. The authors note that CCN concentrations increased in aerosol transported from the Antarctic and Australian continents. This suggests that long-range transport of continental aerosols can effectively influence the entire Southern Ocean south of Australia.
3. As well as influence from the Australian continent, the authors also observed the influence of the Antarctic continent long distances offshore.
4. The authors note the important role the synoptic situation played in mediating aerosol properties during their expedition, especially the role of vertical transport between the marine boundary layer and the free troposphere in enhancing the number of Aitken mode particles.
5. The authors present evidence of a pronounced change in aerosol properties at ∼64° S which they attribute to the transition into the polar atmospheric cell.

Unfortunately, I cannot recommend that this manuscript be accepted for final publication in ACP since in my eyes the scientific significance of the work is quite simply too low. The authors appear to have collected a nice dataset that is nicely presented in a well-written manuscript. However, the authors have essentially not gone beyond describing their measurements. As such, having read the manuscript I was left wondering what I had learned - the conclusions presented above hardly scratch the surface and are essentially well-established. Given this, my recommendation to the authors would be to submit the dataset and accompanying article to a journal for the publication of articles on original research data such as Copernicus's Earth System Science Data journal. If the authors do want to continue to present this research in ACP they need to delve far deeper into interpreting the data and ask themselves what this dataset can contribute that will take the field as a whole forward - in my eyes this goes beyond major revisions.

Author's Answer
The authors appreciate the reviewer's consideration of this manuscript. On reflection, we agree that the scope of the original manuscript was broad and there were considerable opportunities

for more detailed investigation. In response to both reviewers' comments, we have significantly increased the depth and quality of our analysis.

Changes to the analysis include:

- Improved aerosol size distribution mode fitting, including the separation of a nucleation mode throughout much of the voyage
- Modelling of sea salt mass concentrations using a wind speed-dependent model, to allow evaluation of the scaled sea salt measurements obtained from ACSM measurements, and to assess the validity of the model for the conditions observed during this voyage
- Assessing contributions to CCN and the impact of variations in SSA and Aitken mode aerosol concentrations
- Detailed analysis of back trajectories to identify meteorological conditions associated with the above variations in SSA and Aitken mode aerosol

Subsequent to the above changes, we found that the chlorophyll-a exposure over the rasterized productive region (discussed in the original manuscript) was insufficient to explain observed variations in Aitken and nucleation mode aerosol properties. Instead, we have extensively rewritten the manuscript with a greater focus on synoptic-scale meteorological conditions and their key influence on the variability of CCN concentrations in the Southern Ocean.

This has resulted in a much stronger study that highlights the following key findings:

1) Accurate modelling of sea spray aerosol concentrations must be based on detailed air mass meteorological histories, including parameters such as wind speed, rainfall frequency and intensity, and altitude above sea level relative to the marine boundary layer depth. In a dynamic environment like the Southern Ocean, these parameters must be considered along the trajectory of the air mass rather than at the sampling point, and sea spray aerosol are unlikely to reach equilibrium concentrations until the air mass has experienced favourable conditions (low rainfall and low altitudes) for approximately 48 hours.
2) Several periods were identified when CCN concentrations were significantly influenced by either increased wind-related SSA or large-diameter Aitken mode aerosol. Aitken mode aerosol were to be the most significant of these two sources of CCN, potentially providing up to 56% of CCN, even at high latitudes.
3) Despite the high wind speeds associated with frequent cyclonic systems at high latitudes, these weather systems ultimately limited SSA concentrations due to increased rates of precipitation, in-cloud scavenging and vertical transport of air masses into the free troposphere where they became decoupled from the surface source of sea spray. As a result, the highest SSA concentrations and SSA contributions to CCN were observed at lower latitudes.
4) Similarly, while there was frequent evidence of secondary sulfate formation, growth of these aerosol to CCN-relevant diameters was only observed where air masses transited over biologically productive regions at relatively low altitudes, remained within the MBL for 24-48 hours and then encountered a strong cold front which combined rainfall, compression of the MBL and vertical transport into the free troposphere.

Variability arising from subgrid scale meteorology and aerosol properties is poorly represented in current models (Weigum et al., 2016; Lin et al., 2017). This study now provides a detailed examination of the sources of variability in CCN during several episodes of long range transport, sea spray production and secondary aerosol formation, at both high and low latitudes.

We believe this offers valuable insights that will assist in resolving the impacts of synoptic meteorology in models.

Further responses to the reviewer's comments have been included below. Please note that text coloured in red refers to the added text in the manuscript. All page and line numbers refer to the revised manuscript (CWT_Revised_Manuscript_20200501.docx) and supplementary material (CWT_Revised_Supplement_20200501.docx). If the text has been significantly changed, only the section number is given in this document (e.g. "Section 2.1").

General comments

Referee's Comment

1. Page 4, line 5 - In my eyes stating that "the ship and its sampling facilities are discussed in detail" elsewhere is not particularly helpful. I would like to see at least the basic information presented here alongside the data.

Author's Answer

1. The authors acknowledge the benefit of providing this detail in the manuscript and Section 2.1 has been expanded with details of the sampling system layout and conditions within the sampling lines. Details regarding carbon monoxide measurements were added to Section 2.3, and the following clarification was added on Page 4, line 10:

An integrated Nafion membrane drier maintained the was used to relative limit humidity at at < 40 % in the ACSM inlet the ACSM sampling inlet.

Specific comments

Referee's Comment

1. Page 6, line 29 - "...number fraction towards these distributions" would read better as "number fraction towards these sizes".

Author's Answer

1. Section 3.2 has now been extensively rewritten to reflect improvements to the mode fitting process and the above wording has been removed.

Specific comments

Referee's Comment

Page 14 - Although this is perhaps more personal taste, in my view the conclusions section is rather more of a summary. The conclusions of the paper should be more concise than its current form.

Author's Answer

1. The conclusion (Section 5) has been extensively rewritten. The result is more concise and avoids summarizing general observations in favour of restating the key findings

Referee #2

The paper by Alroe et al. reports the result of a Southern Ocean cruise and marine aerosol features from the underexplored region. The paper is fluently written and was a pleasure to read, but unfortunately contains little scientific advancement beyond the current state of knowledge. The results broadly agree very well with the already published papers in the topical area, but I was wondering why the authors did not come up with unique insights possessing a good dataset and all the relevant instruments. Was the study not from the Southern Ocean and without thorough trajectory and ocean colour analysis I would have difficulty recommending it for publication, but I would like to encourage the authors to take a second look at their results and try to enhance the value of the paper by highlighting certain novel aspects. I hope my comments will motivate the authors and may help in improving the paper. For example, were there any oceanographic data available like in-situ chlorophyll measurements to infer phytoplankton blooms or more general tracer measurements by e.g. fluorometer? Last, but not least properly fitted size distributions may help to deepen the discussion of particle sources.

Author's Answer

The authors appreciate the reviewer's comments that have helped us to enhance our investigation and refine the manuscript. On reflection, we agree that the scope of the original manuscript was broad and there were considerable opportunities for more detailed investigation. In response to both reviewers' comments, we have significantly increased the depth and quality of our analysis.

Changes to the analysis include:

- Improved aerosol size distribution mode fitting, including the separation of a nucleation mode throughout much of the voyage
- Modelling of sea salt mass concentrations using a wind speed-dependent model, to allow evaluation of the scaled sea salt measurements obtained from ACSM measurements, and to assess the validity of the model for the conditions observed during this voyage
- Assessing contributions to CCN and the impact of variations in SSA and Aitken mode aerosol concentrations
- Detailed analysis of back trajectories to identify meteorological conditions associated with the above variations in SSA and Aitken mode aerosol

Subsequent to the above changes, we found that the chlorophyll-a exposure over the rasterized productive region (discussed in the original manuscript) was insufficient to explain observed variations in Aitken and nucleation mode aerosol properties. Instead, we have extensively rewritten the manuscript with a greater focus on synoptic-scale meteorological conditions and their key influence on the variability of CCN concentrations in the Southern Ocean.

This has resulted in a much stronger study that highlights the following key findings:

1) Accurate modelling of sea spray aerosol concentrations must be based on detailed air mass meteorological histories, including parameters such as wind speed, rainfall frequency and intensity, and altitude above sea level relative to the marine boundary layer depth. In a dynamic environment like the Southern Ocean, these parameters must be considered along the trajectory of the air mass rather than at the sampling point, and sea spray aerosol are unlikely to reach equilibrium concentrations until the air mass has experienced favourable conditions (low rainfall and low altitudes) for approximately 48 hours.

2) Several periods were identified when CCN concentrations were significantly influenced by either increased wind-related SSA or large-diameter Aitken mode aerosol. Aitken mode aerosol were to be the most significant of these two sources of CCN, potentially providing up to 56% of CCN, even at high latitudes.
3) Despite the high wind speeds associated with frequent cyclonic systems at high latitudes, these weather systems ultimately limited SSA concentrations due to increased rates of precipitation, in-cloud scavenging and vertical transport of air masses into the free troposphere where they became decoupled from the surface source of sea spray. As a result, the highest SSA concentrations and SSA contributions to CCN were observed at lower latitudes.
4) Similarly, while there was frequent evidence of secondary sulfate formation, growth of these aerosol to CCN-relevant diameters was only observed where air masses transited over biologically productive regions at relatively low altitudes, remained within the MBL for 24-48 hours and then encountered a strong cold front which combined rainfall, compression of the MBL and vertical transport into the free troposphere.

Variability arising from subgrid scale meteorology and aerosol properties is poorly represented in current models (Weigum et al., 2016; Lin et al., 2017). This study now provides a detailed examination of the sources of variability in CCN during several episodes of long range transport, sea spray production and secondary aerosol formation, at both high and low latitudes. We believe this offers valuable insights that will assist in resolving the impacts of synoptic meteorology in models.

Further responses to the reviewer's comments have been included below. Please note that text coloured in red refers to the added text in the manuscript. All page and line numbers refer to the revised manuscript (CWT_Revised_Manuscript_20200501.docx) and supplementary material (CWT_Revised_Supplement_20200501.docx). If the text has been significantly changed, only the section number is given in this document (e.g. "Section 2.1").

Key comments

Referee's Comment

1. Were there any oceanographic data available like in-situ chlorophyll measurements to infer phytoplankton blooms or more general tracer measurements by e.g. fluorometer?

Author's Answer

The only in-situ oceanographic measurements included water temperature, salinity and conductivity. Since there were no water chemistry measurements, this study relies on chlorophyll estimates from MODIS-Aqua satellite observations of ocean colour. Usage of sea-surface dimethyl sulfide concentrations from the Surface Ocean Lower Atmosphere Study (SOLAS, Natural Environment Research Council, UK) dataset was also considered, but since this dataset represents a global climatology, it would not have assisted in localizing and assessing specific phytoplankton blooms relevant to this voyage.

Referee's Comment

2. The authors used a sea salt tracer to estimate sea salt mass, but they could also crosscheck with SSA estimated mass and number from recent of earlier sea salt source functions at the observed wind speed. Something more can be done here if proper lab calibrations were not performed for ACSM which would have been very useful given instrumental differences between high resolution AMS used by Ovadnevaite et al. and ToF ACSM used in this study.

Author's Answer

The authors agree that the ACSM measurements of sea salt required further support, given that the instrument was not calibrated for that species. Sea salt mass concentrations have now been estimated using the mass-based sea salt source function given in Ovadnevaite et al. (2012). Section 3.3 has rewritten with full details on how this model was implemented and a comparative evaluation of our observations. In short, it was found that the model offered reasonable agreement for favourable meteorological conditions where the air masses remained within the MBL for at least 48 hours prior to sampling, with rainfall rates below 0.25 mm h^{-1}. However, poor agreement was observed where the above conditions were not met. This suggested that our measurements of sea salt mass were reasonable and permitted increases in sea salt mass concentrations to be correlated against changes in CCN number concentrations. It also highlighted air mass meteorological history as an important consideration when estimating sea spray concentrations from wind speed-dependent models.

Other sea spray source functions were also investigated to model SSA number concentration, specifically those given in Blot et al. (2013) and Norris et al. (2013). Both models predicted unrealistically high SSA concentrations, frequently comparable to or higher than the observed N_{10} concentrations. As discussed in Answer 4 below, an SSA mode could not be fitted to the size distributions, preventing any direct comparison of observed and modelled number concentrations. Therefore, we chose not to pursue this further and have focused our analysis on the mass-based model.

Referee's Comment

3. It is important to realise that the observed particles and their size distributions are a product of cloud cycling. Or in other words, the observed size distribution is a product, not the source for cloud processing. Indeed, all accumulation mode particles can undergo subsequent cloud cycles, but Aitken mode cannot given their modal diameter of 30nm. Bi-modal size distribution has exactly arisen after cloud cycling. If there were no clouds accumulation mode chemical composition would have been entirely made of primary sea salt. As was noted at the beginning properly fitted size distributions (Comments regarding Figure 3) and the above comments may enhance the discussion.

Author's Answer

3. We agree with these comments in general and have applied a more rigorous mode fitting process to separate the cloud-processed Aitken and accumulation modes from relatively unprocessed nucleation mode aerosol. Section 3.2 of the manuscript has been rewritten to reflect the improved mode fitting procedure and detail is also given in Author's Answer 4 below.

Referee's Comment

4. The authors must redo the fitting of log-normal distributions. The shape of "bi-modal" distribution is clearly suggesting more modes, e.g. nucleation mode of ~10nm and second accumulation mode centred at ~420nm. I do not see symmetrical log-normal modes, only one side of them which makes me wondering what the inventive fitting was applied. Specifically, significant departure of log-normal mode from the observed size distribution is suggesting additional mode(s) together with the potentially excessive geometric spread (sigma) above ~1.5. Consequently, nucleation mode is suggesting contribution from new particle formation at the coast or open ocean depending on the trajectories. But first, please do the proper fitting.

Author's Answer

4. The authors agreed that the fitting process could be improved. The original fitting process used a similar process as described in Modini et al. (2015), in which multiple component lognormal modes with unconstrained means are fitted to the distribution. The resulting component modes are then grouped to form each of the expected particle size distribution modes (e.g nucleation, Aitken, accumulation and SSA). However, for this study, it was not possible to fit an SSA mode because the SMPS distributions were limited to maximum diameter of 662 nm. This did not offer enough diameter bins to adequately constrain the SSA mode and separate it from the tail of the larger accumulation mode. In addition, concentrations at the smallest diameters were often noisy. As a result of both limitations, the above unconstrained process often resulted in fitted modes with distribution parameters (mean, spread, amplitude) that did not correspond to physically meaningful modes.

To overcome this, a revised fitting process has been applied and is detailed in Section 3.2. In brief, a maximum of three modes were permitted. Their spread parameters were limited based on values reported in other studies (e.g. (Modini et al., 2015; Fossum et al., 2018) and their means were constrained to diameter ranges that best reflected the nucleation, Aitken and accumulation modes observed in the unfitted distributions (Fig. 2a). Broadening from the SSA mode often became apparent at diameters larger than 300 nm, so fits were only applied to the diameter range 7 – 300 nm to limit this bias. This yielded much improved modal fits (Figs. 4 and S3) and revealed a nucleation mode which was frequently seen in *mSO* air masses. In turn, these new fitted modes have permitted investigation of meteorological conditions and biologically productive regions that favoured strong populations of nucleation mode aerosol, or growth of large diameter Aitken mode aerosol, and their corresponding impact on CCN concentrations (Section 4.2.1, Figs. S5-7).

Minor comments

Referee's Comment

1. Page 4. Line 8. I could not find in this paper nor the referenced paper information about the sampling inlet. Was it community sampling duct of certain dimensions with individual instruments sub-sampling from it? What was the total flow and laminar conditions?
Was it experiencing a significant drying during air passage through it?

Author's Answer

1. The following details regarding the sampling inlet and sample flow conditions have been added to Section 2.1 (Page 3, line 23):

"Aerosol sampling was performed through a common sampling inlet mounted on a mast, located approximately 18 m above sea level at the bow of the ship and co-located with a suite of meteorological instruments. Sample air was drawn through this inlet at a flow rate of approximately 420 L min^{-1}. The sample passed through a 161.5 mm stainless steel tube to a manifold in the bow of the ship, 8 m below the mast in the ship's bow. Most aerosol instruments sampled from this manifold through 3/8" stainless steel tubing. The remaining flow was passed through a 32 mm stainless steel tube to a manifold in a second laboratory and the ACSM sampled from this secondary manifold through 1/4" stainless steel tubing."

There was an ambient temperature differential of up to 25 degrees between the laboratories and the outdoor conditions. The sample air likely underwent significant drying during transit

through the sampling ducts. However, the air temperature in the main sampling laboratory was not accurately controlled or monitored and sample humidity was only measured after the membrane dryers, so the drying effect associated with the temperature change cannot be evaluated separately.

Referee's Comment

2. Page 4, line 24. Was the drier used for ACSM to limit the excessive humidity?

Author's Answer

2. The ACSM is designed with an integrated membrane dryer that was used throughout the voyage. Section 2.2 has been updated with the following text (Page 4, line 10):

"An integrated Nafion membrane drier maintained the relative humidity at <40 % in the ACSM inlet."

Referee's Comment

3. Page 6, line 13. BC threshold was set conservatively in general, however, given pristine nature of the Southern Ocean may have been set even lower, especially as it was an hourly average. Also while number concentration criterion is appropriate, number concentration is not a great arbiter when new particle formation events may increase N10 concentration substantially. It would very useful to present BC data in Figure 2.

Author's Answer

3. The authors agree that high N_{10} concentrations cannot be directly linked to contamination by ship exhaust emissions. After further evaluation, this criterion was found to be unnecessary and has been removed. Likewise, we agree that the Southern Ocean may be expected to have lower BC concentrations than the baseline level used in this study. The MAAP is certainly capable of detecting lower concentrations when using 1-hour averages. Assuming an inverse square relationship between the 95 % confidence interval detection limit and the averaging interval, the detection limit for 1-hour averaged measurements is estimated at 8 ng m^{-3}. However, the goal of this study was not to isolate the most pristine periods, but rather to characterize the conditions commonly present in the Southern Ocean, which include periods influenced by the long-range transport of continental aerosol from major land masses. Therefore the threshold of 30 ng m^{-3} was selected on the basis of BC concentrations reported in other studies of Southern Ocean marine air masses, typically ranging between 1–70 ng m^{-3} (e.g. (Schmale et al., 2019; Humphries et al., 2015; Weller et al., 2013; Kim et al., 2017; Cravigan et al., 2015). This range of values likely reflects differences in instrumentation and sampling location and the selected threshold of 30 ng m^{-3} lies below the midpoint of this range. After applying this threshold, all remaining peaks in BC concentration were examined with respect to wind speed and direction relative to the ship's heading, the path of the associated back trajectories, CO and radon concentrations. In any cases where the ship and air mass trajectories indicated likely contamination, or where CO concentrations were elevated without direct correlation with increased radon concentrations, the associated data was excluded from further analysis. Section 3.1 has been re-written to reflect this reasoning and additional analysis. Also Section 2.3 has been modified to include details regarding the CO measurements (Page 4, line 23):

"Black carbon (BC) and carbon monoxide (CO) concentrations were measured with a Thermo Fisher Scientific 5012 Multi-Angle Absorption Photometer (MAAP) and an Aerodyne

Research Inc. infrared Laser Trace Gas Monitor, respectively. The trace gas monitor was not adequately calibrated and, on average, the CO measurements were 19 ± 5 ppb higher than the estimated reference concentrations given by the Global Greenhouse Gas Reference Network (GLOBALVIEW-CO, 2009). This indicates that the measurements were not quantitatively accurate but correlations between BC and CO were examined when identifying periods contaminated by ship emissions."

Referee's Comment

4. Page 6, line 28. I am confused with this statement as sea spray usually contributes significant number fraction to submicron aerosol based on several established sea spray source functions. Possibly the authors were meant to say that the supermicron sea spray mode contributed a small number fraction to the observed size distributions which would be true.

Author's Answer

4. Section 3.2 has now been extensively rewritten (as discussed in Key Comments Authors Answer 4, above) and this statement has been removed.

Referee's Comment

5. Page 7, line 28. Please provide ranges of temperature and wind speed.

Author's Answer

5. The following details have been added to Section 4.1 (Page 7, line 9):

Throughout the voyage, the median air and sea surface temperatures were 4.7 °C (IQR: 2.9-8.7 °C) and 3.9 °C (IQR: 2.6-8.9 °C), respectively. Median wind speeds observed at the ship were 12.0 m s^{-1} (IQR: 9.5-13.9 ms^{-1})

Referee's Comment

6. Page 8, line 31. Notation is confusing with that of sulfur species. Perhaps is better using upper script notation or mSO-first, mSO-second and so on.

Author's Answer

6. Thank you for this suggestion. The authors agree and this notation has been updated throughout the manuscript using Roman numerals (e.g. *mSO-IV*).

Referee's Comment

7. Page 9, line 5. Why mSO4 is preceding mSO3 period and mSO3 preceding mSO2?

Author's Answer

7. Section 4.2 has been extensively rewritten and now does not discuss each marine air mass as separate cases.

Referee's Comment

8. Page 10, line 19. There is no mention nor reason why CCN not reported for mSO periods.

Author's Answer

8. Section 4.2 has been extensively rewritten with a specific focus on CCN in the marine air masses.

Referee's Comment

9. Page 11, line 29. The only Antarctic terrestrial sources of BC are the scientific bases.

Author's Answer

9. The authors agree and on further investigation, it seems possible that BC was detected from both the Durmont D'Urville research station (6:00 AM on 9th February) and Mawson research station (early on 10th February), due to small peaks in BC concentration as air mass trajectories transitioned westward past these sites. However, these were very brief events and had negligible impact on other aerosol properties. Since the sources of BC in Antarctic air masses are not a major focus of this study, we have removed that comment from Section 4.4.

Referee's Comment

10. Page 12, line 21. This conclusion must be supported by ammonium concentration and degree of neutralisation (DON). There is no mention nor reason of the absence of ammonium concentration. ACSM is perfectly capable of measuring ammonium ion.

Author's Answer

10. While the ACSM is technically capable of measuring ammonium (NH_4), during this voyage, the instrument was configured with a three-stage vacuum system that is less efficient than the more common four-stage system. This lead to increased detection limits for all species. In addition, NH_4 is a relatively "noisy" species due to signal interference with other common species with similar masses, and the mass concentration of non-refractory aerosol in the remote marine environment is typically quite low. As a result, the NH_4 signal was above the detection limit for only 5% of this voyage so it was not feasible to compare the NH_4 concentrations or DON between the air masses.

Referee's Comment

11. Figure 2. BC concentration would be extremely useful on a separate scale of radon graph.

Author's Answer

11. BC concentration has now been added as a third panel in Fig. 2c.

Referee's Comment

12. Table 1. Air mass notations should be spelt below the Table or in the caption. NH4 is an important species discriminating between different neutralisation degrees depending on continental impact. DON could be presented too. DL should be noted below Table or simply like <0.XX

Author's Answer

12. Air mass abbreviations have been defined in the caption for Table 1. Organic aerosol mass and BC detection limits have been specified in the table, as suggested. As discussed in Author's

Answer 10, above, NH4 concentrations were almost constantly below the detection limit and therefore DON could not be calculated. These two parameters have not been presented.

References

Blot, R., Clarke, A. D., Freitag, S., Kapustin, V., Howell, S. G., Jensen, J. B., Shank, L. M., McNaughton, C. S., and Brekhovskikh, V.: Ultrafine sea spray aerosol over the southeastern Pacific: open-ocean contributions to marine boundary layer CCN, Atmos. Chem. Phys., 13, 7263-7278, doi: 10.5194/acp-13-7263-2013, 2013.
Cravigan, L. T., Ristovski, Z., Modini, R. L., Keywood, M. D., and Gras, J. L.: Observation of sea-salt fraction in sub-100 nm diameter particles at Cape Grim, J. Geophys. Res.-Atmos., 120, 1848-1864, doi: 10.1002/2014JD022601, 2015.
Fossum, K. N., Ovadnevaite, J., Ceburnis, D., Dall'Osto, M., Marullo, S., Bellacicco, M., Simó, R., Liu, D., Flynn, M., Zuend, A., and O'Dowd, C.: Summertime Primary and Secondary Contributions to Southern Ocean Cloud Condensation Nuclei, Sci. Rep.-UK, 8, 13844, doi: 10.1038/s41598-018-32047-4, 2018.
GLOBALVIEW-CO: Co-operative Atmospheric Data Integration Project - Carbon Monoxide, CD-ROM, NOAA ESRL, Boulder, Colorado, USA, [Also available on Internet via anonymous FTP to aftp.cmdl.noaa.gov, Path: products/globalview/co], 2009.
Humphries, R. S., Schofield, R., Keywood, M. D., Ward, J., Pierce, J. R., Gionfriddo, C. M., Tate, M. T., Krabbenhoft, D. P., Galbally, I. E., Molloy, S. B., Klekociuk, A. R., Johnston, P. V., Kreher, K., Thomas, A. J., Robinson, A. D., Harris, N. R. P., Johnson, R., and Wilson, S. R.: Boundary layer new particle formation over East Antarctic sea ice – possible Hg-driven nucleation?, Atmos. Chem. Phys., 15, 13339-13364, doi: 10.5194/acp-15-13339-2015, 2015.
Kim, J., Yoon, Y. J., Gim, Y., Kang, H. J., Choi, J. H., Park, K. T., and Lee, B. Y.: Seasonal variations in physical characteristics of aerosol particles at the King Sejong Station, Antarctic Peninsula, Atmos. Chem. Phys., 17, 12985-12999, doi: 10.5194/acp-17-12985-2017, 2017.
Lin, G., Qian, Y., Yan, H., Zhao, C., Ghan, S. J., Easter, R., and Zhang, K.: Quantification of marine aerosol subgrid variability and its correlation with clouds based on high-resolution regional modeling, J. Geophys. Res.-Atmos., 122, 6329-6346, doi: 10.1002/2017jd026567, 2017.
Modini, R. L., Frossard, A. A., Ahlm, L., Russell, L. M., Corrigan, C. E., Roberts, G. C., Hawkins, L. N., Schroder, J. C., Bertram, A. K., Zhao, R., Lee, A. K. Y., Abbatt, J. P. D., Lin, J., Nenes, A., Wang, Z., Wonaschütz, A., Sorooshian, A., Noone, K. J., Jonsson, H., Seinfeld, J. H., Toom-Sauntry, D., Macdonald, A. M., and Leaitch, W. R.: Primary marine aerosol-cloud interactions off the coast of California, J. Geophys. Res.-Atmos., 120, 4282-4303, doi: 10.1002/2014jd022963, 2015.
Norris, S. J., Brooks, I. M., Moat, B. I., Yelland, M. J., de Leeuw, G., Pascal, R. W., and Brooks, B.: Near-surface measurements of sea spray aerosol production over whitecaps in the open ocean, Ocean Sci., 9, 133, doi: http://dx.doi.org/10.5194/os-9-133-2013, 2013.
Ovadnevaite, J., Ceburnis, D., Canagaratna, M., Berresheim, H., Bialek, J., Martucci, G., Worsnop, D. R., and O'Dowd, C.: On the effect of wind speed on submicron sea salt mass concentrations and source fluxes, J. Geophys. Res.-Atmos., 117, doi: 10.1029/2011jd017379, 2012.
Schmale, J., Baccarini, A., Thurnherr, I., Henning, S., Efraim, A., Regayre, L., Bolas, C., Hartmann, M., Welti, A., Lehtipalo, K., Aemisegger, F., Tatzelt, C., Landwehr, S., Modini, R. L., Tummon, F., Johnson, J., Harris, N., Schnaiter, M., Toffoli, A., Derkani, M.,

Bukowiecki, N., Stratmann, F., Dommen, J., Baltensperger, U., Wernli, H., Rosenfeld, D., Gysel-Beer, M., and Carslaw, K.: Overview of the Antarctic Circumnavigation Expedition: Study of Preindustrial-like Aerosols and Their Climate Effects (ACE-SPACE), B. Am. Meteorol. Soc., doi: 10.1175/bams-d-18-0187.1, 2019.
Weigum, N., Schutgens, N., and Stier, P.: Effect of aerosol subgrid variability on aerosol optical depth and cloud condensation nuclei: implications for global aerosol modelling, Atmos. Chem. Phys., 16, 13619-13639, doi: 10.5194/acp-16-13619-2016, 2016.
Weller, R., Minikin, A., Petzold, A., Wagenbach, D., and König-Langlo, G.: Characterization of long-term and seasonal variations of black carbon (BC) concentrations at Neumayer, Antarctica, Atmos. Chem. Phys., 13, 1579-1590, doi: 10.5194/acp-13-1579-2013, 2013.

Marine productivity and synoptic meteorology drive summer-time variability in Southern Ocean aerosols

Joel Alroe[1], Luke T. Cravigan[1], Branka Miljevic[1], Graham R. Johnson[1], Paul Selleck[2], Ruhi S. Humphries[2], Melita D. Keywood[2], Scott D. Chambers[3], Alastair G. Williams[3] and Zoran D. Ristovski[1]

[1]School of Chemistry, Physics and Mechanical Engineering, Queensland University of Technology, Brisbane, Australia
[2]Climate Science Centre, CSIRO Oceans and Atmosphere, Aspendale, Australia
[3]Environmental Research, ANSTO, Lucas Heights, Australia

Correspondence to: Zoran D. Ristovski (z.ristovski@qut.edu.au)

Abstract

Cloud-radiation interactions over the Southern Ocean are not well constrained in climate models, in part due to uncertainties in the sources, concentrations and cloud-forming potential of aerosol in this region. To date, most studies in this region have reported measurements from fixed terrestrial stations or a limited set of instrumentation, and often present findings as broad seasonal or latitudinal trends. Here, we present an extensive set of aerosol and meteorological observations obtained during an austral summer cruise across the full width of the Southern Ocean south of Australia. Three episodes of continental-influenced air masses were identified, including an apparent transition between the Ferrel atmospheric cell and the polar cell at approximately 64° S, and accompanied by the highest median cloud condensation nuclei (CCN) concentrations, at 252 cm^{-3}. During the other two episodes, synoptic-scale weather patterns diverted air masses across distances greater than 1000 km from the Australian and Antarctic coastlines, respectively, indicating that a large proportion of the Southern Ocean may be periodically influenced by continental air masses. In all three cases, a highly cloud-active accumulation mode dominated the size distribution, with up to 93 % of the total number concentration activating as cloud condensation nuclei. Contrary to modelled predictions, frequent storm activity inhibited sea spray aerosol concentrations, while the highest concentrations and largest influence on CCN were observed at lower latitudes with comparatively stable, dry weather conditions. However, CCN concentrations were more strongly impacted by high concentrations of large-diameter Aitken mode aerosol in air masses which passed over regions of elevated marine biological productivity, potentially contributing up to 56% of the cloud condensation nuclei concentration. Weather systems were vital for aerosol growth in biologically-influenced air masses and in their absence ultrafine aerosol diameters were less than 30 nm. These results demonstrate that air mass meteorological history must be considered when modelling sea spray concentrations and highlight the potential importance of subgrid scale variability when modelling atmospheric conditions in the remote Southern Ocean.~~In contrast, sampling periods influenced by marine air masses frequently demonstrated a correlation between air mass trajectories over regions of high biological productivity and subsequent enhancement of an Aitken mode centred at approximately 30 nm and contributing an average of 71% of the total aerosol number concentration. Although these small diameters limited their contribution to cloud condensation nuclei concentrations,~~

~~Aitken number concentrations and diameters were highly variable. A detailed investigation of the marine air masses revealed that this variability may be attributed to the availability of biogenic precursors, the competing influence of condensation sinks (such as sea spray aerosol) and vertical transport between the marine boundary layer and the free troposphere. This variability of the marine Aitken mode as well as the instances of long-range transport were governed by synoptic-scale weather systems, through their influence on air mass trajectories and both generation and depletion of condensation sinks. These results demonstrate the highly dynamic nature of Southern Ocean aerosol and their complex dependence on both biological productivity and synoptic-scale weather systems.~~

1 Introduction

Aerosols have an important role in radiative forcing both through direct absorption and scattering of incident solar radiation and through their indirect effects on cloud formation, structure and lifetime (Haywood and Boucher, 2000; Albrecht, 1989). However, they have been identified as the largest source of uncertainty in the global radiation budget (Myhre et al., 2013). Oceans cover 70 % of the Earth's surface and thus aerosols within the marine environment are of particular importance for climate models. To illustrate this, Rosenfeld et al. (2019) recently proposed that 75 % of the uncertainty in the cooling effect of marine boundary layer (MBL) clouds may be associated with the influence of aerosols on cloud area and lifetime. General circulation models exhibit persistent biases in the levels of cloud-based radiative forcing estimated for the Southern Ocean, with insufficient reflected shortwave radiation particularly occurring behind cold fronts and during the austral summer (Williams et al., 2013; Protat et al., 2017).

The Southern Ocean receives minimal anthropogenic influence, so the relatively pristine conditions offer a valuable opportunity to investigate the interlinked atmospheric and oceanic processes that govern the natural marine environment. The main sources of aerosol to the Southern Ocean boundary layer are well known and include sea spray aerosol (SSA) generated from wind shear and bubble bursting, non-sea salt sulfates (nss-SO_4) formed from the condensation of volatile biogenic precursor gases, and the long range transport of anthropogenic shipping emissions or continental aerosols from the surrounding land masses. However due to its vast extent and the logistical challenges involved with performing in-situ measurements in such remote and harsh conditions, observations from this region are very limited. To address this gap, recent years have seen a surge in sampling expeditions (e.g. Fossum et al., 2018; O'Shea et al., 2017; Stephens et al., 2018; Protat et al., 2017; Schmale et al., 2019; Dall'Osto et al., 2017; Humphries et al., 2016) ~~(Fossum et al., 2018)Fossum et al., 2018;(O'Shea et al., 2017) O'Shea et al., 2017; (Stephens et al., 2018)Stephens et al., 2018;(Protat et al., 2017) Protat et al., 2017; (Schmale et al., 2019)Schmale et al.;(Dall'Osto et al., 2017) Dall'Osto et al., 2017; (Humphries et al., 2016)Humphries et al., 2016)~~ with a focus on quantifying the aerosol production sources in this region and their contribution to cloud condensation nuclei (CCN).

The Southern Ocean represents a wide band of open ocean that encircles the globe between approximately 40–70° S and is largely uninterrupted by land masses. Its location, straddling the transition between the Ferrel and Polar atmospheric circulation cells, gives rise to a relentless eastward procession of cyclonic low-pressure systems, which particularly develop in the southern

Indian Ocean and to the south of Australia (Simmonds et al., 2003). Their associated high wind speeds and wave heights promote the generation of SSA, which contribute a major fraction of the global aerosol mass loading (Vignati et al., 2010). SSA are composed of an internal mixture of inorganic salts and biogenic organic material (Cravigan et al., 2019; Ault et al., 2013). Typically they form coarse-mode aerosol with mean diameters in the range of approximately 200–500 nm (Quinn et al., 2017; Lewis et al., 2004), although substantial number concentrations have been observed at smaller sizes, containing enhanced organic fractions (Andreae and Rosenfeld, 2008). Due to both their size and hygroscopic nature, these aerosols are highly effective cloud condensation nuclei (CCN), rapidly adsorbing water to activate as cloud droplets when exposed to relatively low water supersaturations (SS). These same properties limit their lifetime in the marine boundary layer, leading to relatively low number concentrations. In turn, they often represent a small fraction of total CCN concentrations. However recent studies from the Southern Ocean have reported significant and varied SSA contributions to CCN number concentrations of between 19–32 % at 0.15 % SS (Schmale et al.), up to 65 % at 0.1 % SS (Quinn et al., 2017) and 60–100 % at <0.32 % SS (Fossum et al., 2018). These inconsistent and widely spread results illustrate the need for further investigation into the causes of this variability.

In addition to tempestuous atmospheric conditions, the Southern Ocean also hosts extensive upwelling of nutrient-rich waters along the Antarctic coastline and the Antarctic Convergence. The high levels of biological activity in these locations generates an increased flux of dimethyl sulfide (DMS) into the atmosphere, with the potential for increased production of nss-SO_4 or methanesulfonic acid (MSA) aerosol (Simpson et al., 2014). This nss-SO_4 production depends significantly on precursor concentrations and favourable meteorological conditions (Bianchi et al., 2016), while the resulting size distribution of nss-SO_4 aerosol is affected by the surface area concentration of other aerosols that can act as condensation sinks (O'Dowd and de Leeuw, 2007). In both the tropics and the Southern Ocean, cloud-based convective transport of air masses into the free troposphere has been shown to result in new particle formation (NPF) (Clarke et al., 1998; Williamson et al., 2019). The colder air temperatures of the free troposphere promote partitioning into the aerosol phase, while the in-cloud wet scavenging of CCN removes competing condensation sinks. Depending on the precursor concentrations, when entrained back into the MBL in the cloud outflow regions, these newly formed aerosol can greatly increase nucleation or even Aitken mode aerosol number concentrations~~primarily contribute to Aitken mode number concentrations~~. Conversely, if meteorological conditions do not support this vertical transport and removal of condensation sinks, any nss-SO_4 is more likely to partition to existing aerosol, increasing the mean size of the aerosol distribution.

The strong weather systems present in the Southern Ocean could be expected to promote NPF. In support for this, Fossum et al. (2018) reported Aitken mode number concentrations that were substantially higher than the accumulation mode in characteristic Southern Ocean air masses, while the reverse was true for air masses from the Antarctic continent. Conversely, Dall'Osto et al. (2017) and Humphries et al. (2016) both reported episodes of nucleation mode aerosol concentrations that were three times higher within the sea ice zone than from the open ocean. In the latter case, the air mass originated in the Antarctic free troposphere and as such, the precursor source was not immediately apparent. Throughout two thirds of their circumnavigation of Antarctica, Schmale et al. (2019) observed slightly higher aerosol number concentrations for aerosol with

diameters smaller than 80 nm. However, since the observations were averaged across each leg of the voyage, it is difficult to directly examine the impact of changes in air mass or meteorological conditions.

These discrepancies do not stop at physical observations. Current global climate models operate over spatial grids that can span hundreds of kilometres per grid box and subgrid variability within these boxes can significantly limit the accuracy of the model, particularly for aerosol parameters such as CCN (Lin et al., 2017; Weigum et al., 2016). Given the highly dynamic conditions within the Southern Ocean, and the limited and sometimes conflicting observations reported to date, further investigation is required to identify the main factors contributing to aerosol variability.

This study presents in-situ aerosol and meteorological measurements from the Cold Water Trial (CWT) voyage ~~taken~~ in the austral summer over a full latitudinal transect of the Southern Ocean, between Hobart, Australia and the marginal ice zone. To our knowledge, it represents the first comprehensive dataset focused on this region of the Southern Ocean. We examine characteristic changes in the aerosol number size distribution and identify air masses or aerosol sources that likely contributed to these changes. In particular, we examine the variation in CCN concentrations between each air mass and investigate the contributing sources. ~~These include a region of increased biological productivity that is shown to be frequently associated with changes in the concentration and size of Aitken mode aerosol. In addition, s~~Several episodes of long-range transport of continental aerosol are identified. Ultimately, we show that synoptic-scale weather systems both directly and indirectly have an important influence on aerosol properties by promoting or inhibiting SSA and secondary aerosol generation.~~, complicating attempts to correlate CCN concentrations with other observations.~~

2 Measurements

2.~~2~~ 1 Voyage overview

The measurements were conducted during the first cruise of *RV Investigator* into polar waters, over a three-week period from January – February 2015. The ship travelled southward from Hobart to the marginal ice zone, primarily along the 146th line of longitude, reaching a maximum latitude of 65° S before returning along a similar course (Fig. 1). Aerosol sampling was performed through a common sampling inlet mounted on a mast, located approximately 18 m above sea level at the bow of the ship and co-located with a suite of meteorological instruments. Sample air was drawn through this inlet at a flow rate of approximately 420 L min^{-1}. The sample passed through a 161.5 mm stainless steel tube to a manifold in the bow of the ship, 8 m below the mast in the ship's bow. Most aerosol instruments sampled from this manifold through 3/8" stainless steel tubing. The remaining flow was passed through a 32 mm stainless steel tube to a manifold in a second laboratory and the ACSM sampled from this secondary manifold through 1/4" stainless steel tubing.

Additional details regarding this ~~The~~ ship and its sampling facilities are discussed in ~~more detail in (Humphries et al., 2019)~~Humphries et al. (2019). As this was a trial voyage of a new research vessel, navigational records are unavailable for

several periods of up to 18 hours. Location coordinates were interpolated assuming a constant ship velocity throughout these times.

2.2 Primary in situ measurements

Aerosol size distributions were measured over the diameter range 4 – 673 nm with two TSI 3080 Scanning Mobility Particle Sizers (SMPS). One was configured with a TSI 3085 Nano Differential Mobility Analyser (DMA) and a TSI 3776 Ultrafine Condensation Particle Counter (CPC), while the other used a TSI 3081 Long DMA and TSI 3010 CPC. The combined sample flow rate was 2.5 L min^{-1} and was dried with a membrane dryer (Nafion MD-700) upstream of both instruments. Size distributions were obtained with a time resolution of 5 minutes.

For comparison, a Neutral Cluster and Air Ion Spectrometer (NAIS) was used to obtain size distributions of ultrafine aerosol with diameters between 2–42 nm. The lower size limit offered by this instrument makes it well suited for observing aerosol nucleation events and any subsequent growth of the newly formed aerosol into the Aitken size range. The NAIS was operated with a 4 min time resolution and a sample flow rate of 60 L min^{-1} to minimise diffusional losses. No sample drying was applied for this instrument due to the high flow rate.

Cloud condensation nuclei (CCN) concentrations were measured with a Droplet Measurement Technologies single growth column CCN counter (Model CCN-100), operated at a supersaturation (SS) of 0.5 %. For comparison, total number concentrations (N_{10}) of aerosol with diameters larger than 10 nm were measured with a TSI 3772 CPC.

Chemical analysis of non-refractory submicron aerosol was generated by an Aerodyne Time of Flight Aerosol Chemical Speciation Monitor (ACSM) and a full description of its design and operation is given in ~~Fröhlich et al. (2013)~~ Fröhlich et al. (2013). An integrated Nafion membrane drier maintained the relative humidity at <40 % in the ACSM inlet. Measurements were averaged to a 1-hour time resolution and a collection efficiency of 1 was applied to reflect high aerosol acidity observed throughout the voyage. The instrument's size-dependent inlet transmission is at a maximum for vacuum aerodynamic diameters between 100–450 nm (Jayne et al., 2000; Liu et al., 2007) and therefore the composition measurements best represent primary marine aerosol and accumulation mode aerosol.

~~Sea spray aerosol (~~SSA~~) and MSA are two components of particular interest in marine studies that~~ can be challenging to quantify from ACSM measurements. Most compounds present in SSA are refractory and are not efficiently vaporised in the ACSM. Since NaCl is typically the most abundant compound, Ovadnevaite et al. (2012)~~SSA concentrations have been estimated from the NaCl+ ion signal using the scaling factor proposed by Ovadnevaite et al. (2012).~~ demonstrated that the NaCl+ ion signal could be used to estimate sea salt mass concentrations by applying a scaling factor of 51. The same scaling factor has been used in this study since there were no independent measures of sea salt mass concentration and the ACSM was not calibrated against sea salt or a NaCl laboratory standard. In Sect. 3.3, as an alternate evaluation of the scaling factor, the resulting sea salt concentrations have been contrasted against modelled values derived from wind speed.~~Where possible, the mass concentration of MSA was separated from other organic and sulfate species via modifications to the fragmentation table,~~

~~determined by Langley et al. (2010). Low aerosol mass concentrations often inhibited this approach, yielding MSA concentrations below the detection limit. Organic and sulfate mass concentrations should be assumed to include MSA unless otherwise specified. Furthermore, both the MSA fragmentation table changes and the SSA scaling factor were not calibrated against laboratory standards, so these concentrations are discussed as qualitative estimates only.~~

~~Aerosol hygroscopicity and volatility were measured with a Volatility and Hygroscopicity Tandem Differential Mobility Analyser (VH-TDMA). The instrument is discussed in detail in Fletcher et al. (2007). The sample flow was dried with a membrane dryer (Nafion MD-700) to lower than 30 % relative humidity. An automated valve system was installed in the sample line to allow every second measurement to be acquired through a thermodenuder, which was heated to 120 °C. Measurements were made for pre-selected aerosol with dry mobility diameters of 40, 100 and 150 nm, and each full cycle of heated and unheated measurements was acquired at an 18 minute time resolution. Hygroscopic growth factors were obtained at 90 % relative humidity. These have been converted to the hygroscopicity parameter, κ, defined via the κ- Köhler theory (Petters and Kreidenweis, 2007):~~

$$\kappa = \left[\frac{\exp\left(\frac{4\sigma M_w}{HGF\,\rho_w D R T}\right)}{RH/100} - 1\right](HGF^3 - 1),$$

~~Where σ is the droplet surface tension, M_w is the molecular mass of water, ρ_w is the density of water, D is the dry aerosol diameter, R is the ideal gas constant, T and RH are the set temperature and relative humidity within the aerosol humidifier. In this study, the surface tension of water has been used ($\sigma = 0.072$ J m^{-2}).~~

2.3 Supporting measurements

Black carbon (BC) and carbon monoxide (CO) concentrations were measured with a Thermo Fisher Scientific 5012 Multi-Angle Absorption Photometer (MAAP) and an Aerodyne Research Inc. infrared Laser Trace Gas Monitor, respectively. The trace gas monitor was not adequately calibrated and, on average, the CO measurements were 19 ± 5 ppb higher than the estimated reference concentrations given by the Global Greenhouse Gas Reference Network (GLOBALVIEW-CO, 2009). This indicates that the measurements were not quantitatively accurate but correlations between BC and CO were examined when identifying periods contaminated by ship emissions.~~A Thermo Fisher Scientific 5012 Multi-Angle Absorption Photometer was used to measure black carbon (BC) mass concentrations, an important marker for ship exhaust and other anthropogenic combustion sources.~~ Atmospheric radon concentrations were obtained from a 700 L dual-flow-loop two-filter radon detector, described in Chambers et al. (2018), providing a signature of air masses that have passed over land. ~~Ocean s~~Sea- surface chlorophyll-a (Chl-a) concentrations were sourced from the MODIS-Aqua Level-3 Binned dataset maintained by the NASA Goddard Space Flight Centre Ocean Biology Processing Group (OBPG, 2018). These represent monthly-average sea surface concentrations at 4-km spatial resolution.

Seven-day backward air mass trajectories were estimated using the HYSPLIT Lagrangian dispersion model (Stein et al., 2015). The modelled trajectories were based on Global Data Assimilation System (GDAS) meteorological data, gridded at a 1° spatial resolution. Back trajectories were obtained for each hour of the voyage, and associated parameters were recorded including surface Chl-a, rainfall and air mass altitude relative to the boundary layer mixing height (e.g. Fig. S1). The accuracy of these back trajectories are inherently restricted by the accuracy of the model and the limited spatial and temporal resolution of the underlying meteorological data. In light of this, ensembles of 27 trajectories have been obtained for each hour of the voyage. The HYSPLIT modelling system generates ensembles by applying spatial offsets to the meteorology for each trajectory (Draxler, 2003). The offset is approximately 250 m in the vertical direction, so all trajectories were propagated from this initial altitude above sea level. The median boundary layer depth was 1200 m along the voyage track, so it has been assumed that trajectories initiated at an altitude of 250 m offer a reasonable representation of the air masses sampled at the ship, within the limitations of the model. For each ensemble, all associated parameters were averaged at each time step along the back trajectory as a best estimate of the air mass position and conditions. In support of the back trajectories and for identification of synoptic weather systems, mean sea level pressure charts were accessed from the Australian Bureau of Meteorology weather maps archive.

3 Data analysis

3.1 Identification of ship emissions

Due to the position of the sampling inlet at the bow of the ship, gas and particle phase measurements were excluded where wind directions were from the rear of the ship, defined as between 120–240° relative to the ship's heading. Further contamination from ship exhaust was identified by applying a 1-hour rolling mean to the BC concentrations. At this time resolution, the MAAP had a nominal detection limit of 8 ng m^{-3} and clean marine air masses often exhibited concentrations below this limit (Fig. 2c). Since the aim of this study was to assess the characteristic air masses present in the Southern Ocean, data was excluded where the 1-hour mean concentration was above 30 ng m^{-3}, where the 1-minute BC concentration was above 150 ng m^{-3} or where the air mass back trajectories crossed the ship's path and may have captured its plume. Other studies have reported BC concentrations from Southern Ocean air masses that range between 1–70 ng m-3 (Cravigan et al., 2015; Kim et al., 2017; Humphries et al., 2019; Schmale et al., 2019). Therefore the selected limit was well within this range and allowed periods associated with long-range transport of continental air masses to be retained, while minimising local contamination from the ship. After applying the above thresholds, the remaining BC measurements were manually assessed for correlation with radon and CO, which were treated as proxies for continental emissions and local combustion respectively. ~~Periods impacted by ship exhaust have been excluded from the dataset. These were identified by 1-minute BC concentrations above 150 ng m^{-3}, hourly-average BC concentrations above 30 ng m^{-3} or N_{10} number concentrations greater than 5000 cm^{-3}. Due to~~

~~the position of the sampling inlet at the bow of the ship, data were also excluded where wind directions were from the rear of the ship, defined as between 120–240° relative to the ship's heading.~~

3.2 Particle diameter mode fits

A modified version of the lognormal mode fitting scheme discussed in ~~Modini et al. (2015)~~ Modini et al. (2015) was applied to the 1-hour average particle size distributions. The characteristic SSA mode is typically very broad and significantly overlaps the accumulation mode (Quinn et al., 2017). For this reason, the SSA mode is usually fit based on aerosol with diameters >500 nm, to minimise bias from the accumulation mode. In this study, size distributions were measured to a maximum diameter of 673 nm, so it was not possible to adequately constrain the SSA mode.

After removing ship-contaminated measurements, the remaining distributions often exhibited local minima at 30 and 80 nm, separating peaks corresponding to the nucleation, Aitken and accumulation modes. Up to three lognormal modes were fitted using the above minima as bounds for the respective means and their spread was limited to the range 1.1 – 1.7, or 1.1 – 1.5 for the nucleation mode. At diameters <7 nm the distributions became persistently noisy due to low particle counts, while at diameters >300 nm the distributions were often broadened by contributions from SSA aerosol. These diameter ranges were excluded from the fitting process. The mode fitting was performed using the "minpack.lm" non-linear least squares minimisation package in the R software environment (Scrucca et al., 2016). In each case, the number of fitted modes was selected using the Bayesian Information Criterion, an estimator of model accuracy that penalises the complexity of the model to avoid overfitting.

In some cases, the fitted nucleation mode became sufficiently broad or exhibited mean diameters that prevented meaningful separation of the Aitken and nucleation modes. In these cases, both modes were combined and assigned to the nucleation or Aitken mode, dependent on whether the combined peak diameter was larger or smaller than 30 nm. In this study, both modes will be collectively termed ultrafine aerosol when distinguishing them from accumulation mode aerosol or SSA.

As will be discussed in Sect. 4.2.1, the volume concentration of the Aitken mode aerosol can be a useful predictor of their contribution to $CCN_{0.5\%}$ number concentrations. At the Aitken size range, aerosol number concentrations are poorly correlated with CCN because CCN activation potential is strongly dependent on particle size (Dusek et al., 2006). In contrast, the aerosol volume concentration weights the number concentration with a cubic dependence on particle diameter, devaluing contributions from small diameter aerosol that are less likely to have a role as CCN. These volume concentrations were determined by integrating over both the Aitken and nucleation modes in the number size distribution, assuming spherical-shaped aerosol. The nucleation mode was included to account for the periods when the two modes could not be adequately separated but where their combined mode extended into CCN-relevant sizes.~~The SMPS size distributions were averaged to a 2-hour time base and up to nine lognormal modes were fitted to each distribution using the "Mclust" finite mixture modelling package in the R software environment (Scrucca et al., 2016). This process used the Bayesian Information Criterion, an estimator of model accuracy that penalises the complexity of the model to avoid overfitting. These modes were then grouped under two particle~~

~~size distributions modes, representing Aitken and accumulation mode aerosol, respectively. The fitted modes were allocated according to their position above or below the Hoppel minimum, defined as the diameter bin corresponding to the minimum number concentration between 40–100 nm. To aid in selecting the most representative local minimum within this range, the SMPS distributions were smoothed using a rolling average across the diameter bins, with a 6-bin averaging window. Representative modal diameters for the aggregated Aitken and accumulation distributions were calculated from their respective geometric means. Since the distributions were limited to a maximum diameter of 660 nm, there were insufficient diameter bins above 500 nm to adequately constrain an additional primary marine aerosol mode. As such, it should be noted that primary marine aerosol contributes some small but undetermined number fraction towards these distributions.~~

3.3 Evaluation of SSA measurements ~~Classification of air masses~~

There were no independent measures of sea salt mass concentration and the ACSM was not calibrated against laboratory standards for this species. So to evaluate the suitability of the $NaCl^+$ scaling factor (see Sect. 2.2), the sea salt mass concentrations were estimated using the sea salt source function given by Ovadnevaite et al. (2012). This source function was developed based on measurements from an Aerodyne High Resolution Time of Flight Aerosol Mass Spectrometer, employing the same approach for scaling the $NaCl^+$ signal. While the ACSM does not share the same resolution, the two instruments are otherwise highly similar making this source function the most ideally suited for comparison with the ACSM measurements.

The source function depends on the sea-surface mass flux of submicron sea salt in ng m^{-2}, given as a function of wind speed (U_{10}) at 10 m above sea level and for $U_{10} \geq 3.7$ m s^{-1}. At wind speeds below this limit, the flux is assumed to be zero due to a lack of whitecapping (Callaghan et al., 2008).

Ovadnevaite et al. (2012) observed decreased sea salt fluxes during periods of increasing wind speeds and increased flux for decreasing wind speeds. As a result, the authors presented separate wind-dependent flux parameterisations for each case, and the following parameterisation based on the total dataset with no differentiation between increasing or decreasing wind speed:

$$F = 0.003 \times U_{10}^{2.7} + 0.47 \quad (1)$$

The resulting submicron sea salt mass concentration (C_{SS}) was then given by:

$$C_{SS} = \frac{F \times t}{H_{MBL}} \quad (2)$$

H_{MBL} is the marine boundary layer height in metres, and t is the filling time in seconds. Ovadnevaite et al. (2012) found that a 2-day filling time gave the best agreement. This reflected the approximate frequency of passing synoptic systems or changes in air mass observed during the CWT cruise, so in this study the filling time was taken to be the time since the air mass last subsided from the free troposphere into the MBL prior to reaching the ship, up to a maximum of 48 hours. Over the same time interval, U_{10} was taken to be the surface wind speed at each hour along the air mass trajectory, to reflect the wind conditions where the aerosol production was taking place.

The sea salt concentrations modelled with Eq. (1) overpredicted the observed data in most cases, but broadly reproduced many of the trends (Fig. S2). The worst predictions occurred when there was substantial rainfall during the 48-hour fill time. In

contrast, the best agreement was found during the final 3.5 days of the cruise, where sea salt concentrations were high and air masses experienced stable dry conditions within the MBL for >48 hours prior to reaching the ship. During this period, the modelled concentrations overpredicted the in-situ measurements by 49 %, on average.

The sea salt flux parameterisation for decreasing wind speed was disregarded since it would have further inflated the model concentrations. Much better agreement was obtained using the parameterisation corresponding to increasing wind speeds, which overestimated the observed concentrations by only 4 %, on average (Fig. S2). Given this close agreement during ideal conditions for SSA production, the modelled results offer support for the accuracy of the scaled sea salt measurements.

~~There were few instances of "steady state" conditions in which the aerosol properties remained largely unchanged over extended periods of time. However, on several instances, the aerosol size distribution became significantly biased towards either the Aitken or accumulation mode and the modal diameters abruptly shifted. The rapid onset of these changes suggested a change in air mass origins. The likely sources of these distinct air masses or aerosol production sources were investigated by examining the corresponding air mass back trajectories, radon concentrations and the associated aerosol chemical composition.~~

3.4 Classification of air masses ~~Rasterization of productive region~~

There were few instances of "steady-state" conditions in which the aerosol properties remained largely unchanged over extended periods of time. However, on several instances, the aerosol size distribution became significantly biased towards either the Aitken or accumulation mode and the modal diameters abruptly shifted. The rapid onset of these changes suggested a change in air mass origins. The likely sources of these distinct air masses or aerosol production sources were investigated by examining the corresponding air mass back trajectories, radon concentrations and the associated aerosol chemical composition.~~The maps of oceanic Chl-a indicated numerous areas of elevated biological productivity during the austral summer. Aside from the nutrient-rich Antarctic coastal waters, the highest concentrations were seen in a broad region stretching southwards from the Kerguelen Plateau to Antarctica (Fig. 1). Due to the prevailing direction of air masses, this region was viewed as a likely source for precursors of NPF and modification of existing aerosol populations. The 4 km resolution of the Chl-a concentrations was beyond the spatial accuracy of the air mass paths estimated with HYSPLIT. To aid identification of air masses which had a higher likelihood of being influenced by biological activity, the productive Kerguelen-Antarctic region was subdivided into a grid of 3 x 6 cells, using an equirectangular projection. Chl-a concentrations were averaged within each cell. In order to specifically target high Chl-a concentrations, a threshold was applied to disregard any cells with monthly-average concentrations lower than 150 % of the mean for the whole rasterized region. The southern most row of cells substantially overlaps the Antarctic coastline and is therefore only relevant to air masses that pass over a comparatively narrow band of ocean. This was intentionally chosen to ensure that the highly productive Prydz Bay was included, and to provide latitudinal constraints for the high concentrations along the coastline, reducing their bias on the typically lower concentrations seen further from the coast.~~

~~The gridded and thresholded region was subsequently used to calculate the proportion of each back trajectory that passed through highly productive cells while within the marine boundary layer. A proxy for the cumulative exposure to biogenic emissions was also estimated from the product of the time that an air mass back trajectory spent in the MBL over each productive cell and the corresponding cell-averaged Chl-a concentration.~~

4 Results and discussion

4.1 General observations

Throughout the voyage, the median air and sea surface temperatures were 4.7 °C (IQR: 2.9-8.7 °C) and 3.9 °C (IQR: 2.6-8.9 °C), respectively. Median wind speeds observed at the ship were 12.0 m s^{-1} (IQR: 9.5-13.9 ms^{-1}) and frequent synoptic-scale weather systems were observed passing the ship throughout the voyage, particularly at latitudes south of 50° S.

As shown in Fig. 1, the sea surface Chl-a concentrations indicated several regions of elevated biological productivity in this sector of the Southern Ocean. The most intense concentrations were localised along the Antarctic coastline, however significantly elevated concentrations were also located near the Kerguelen Plateau. This is an underwater volcanic plateau in the vicinity of the Kerguelen, Heard and McDonald Islands, that acts as a hotspot for marine biological activity during the austral summer months.

Throughout the voyage, $CCN_{0.5\%}$ concentrations were strongly variable (Fig. S3b), with an overall mean of 189 ± 65 cm^{-3}. To examine the sources of this variability, it is helpful to consider the particle size distributions shown in Fig. 2(a). The highest total aerosol number concentrations and the greatest number contributions from Aitken and nucleation mode aerosol, were typically associated with maritime Southern Ocean (*mSO*) air masses. ~~Relatively warm conditions were experienced throughout the voyage with minimum air and sea surface temperatures of 2.7 and 0.8 °C, respectively. At the ship, mean wind speeds were 11.6 m s^{-1} and frequent synoptic scale weather systems were observed passing the ship throughout the voyage, particularly at latitudes greater than 50° S.~~

~~A time series of particle size distributions is shown in Fig. 2(a). The Aitken mode aerosol represented the greater proportion of the total aerosol number throughout most of the voyage, with a geometric mean diameter frequently as low as 20 nm.~~ These periods were often characterised by ~~are attributed to maritime Southern Ocean (*mSO*) air masses, with typically~~ long fetches over the open ocean to the south west and radon concentrations which averaged 43 ± 17 mBq m^{-3}, in good agreement with the Southern Ocean background concentration of 50 mBq m^{-3} given in Chambers et al. (2018).

The long south-westerly fetches were frequently disrupted by the passage of synoptic and mesoscale weather systems. This was notably observed on 4^{th} – 6^{th}, 8^{th} – 9^{th} and on 11^{th} February. On all three occasions, the aerosol number concentrations decreased, the size distributions became biased towards the accumulation mode and radon concentrations increased above the marine background (Fig. 2). Air mass trajectories and radon concentrations indicated that the first period was influenced by continental and coastal Australian air masses (*cAU*), while the latter two received air masses from continental Antarctica (*cAA*).

~~The mean a~~Aerosol properties observed from each air mass are shown in ~~Table 1~~Table 1. They are further subdivided into discrete episodes for each air mass in Table S1 and are discussed in detail in the following sections.

4.2 Characteristics of the *mSO* air mass

Across the four *mSO* sampling periods, the mean N_{10} concentration of 540 ± 200 cm^{-3} ~~541 cm^{-3}~~ was almost double the concentrations observed from the continental air masses. Schmale et al. (2019) reported a similar relative change in number concentration between measurements in the mid-latitudes of the Southern Ocean and those taken close to the Antarctic continent during the ACE-SPACE circumnavigation of Antarctica. ~~This~~ The difference was driven by ~~a~~ substantially higher Aitken and nucleation mode fractions~~fraction, representing up to 94 % of the total number concentration~~, as shown in Fig. 3. On average, 57% of non-SSA aerosol in the *mSO* air mass was attributed to the nucleation mode and this increased to over 90% during a brief intense burst of nucleation mode aerosol on 6th February 2015. The marine nucleation and Aitken mode aerosol concentrations were highly variable, rarely remaining constant for more than a few hours at a time (Fig. 4). The NAIS particle spectra did not reveal any instances of newly-formed sub-10 nm particles growing into the nucleation range, so the NPF events must have occurred some distance from the ship. At a mean of 26 nm, nucleation mode aerosol were typically at least twice as large as in the continental air masses, at times transitioning into the Aitken size range (Fig. S3) and suggesting a greater availability of aerosol precursors during NPF events or increased condensational growth associated with these marine air masses.

For comparison, similar short-lived sub-20 nm modes were reported by Covert et al. (1996) and Bates et al. (1998) during austral summer voyages in the Pacific and Australian sectors of the Southern Ocean, respectively. In the latter case, nucleation mode concentrations typically did not exceed those of the Aitken mode. However their cruise did not extend to latitudes south of 55 °S and this reflects the latitudinal distribution of Aitken contributions observed during the CWT cruise. In contrast, during a concurrent cruise in 2015 through the Atlantic sector of the Southern Ocean, Fossum et al. (2018) did not observe a significant proportion of nucleation mode aerosol in most marine air masses and saw minimal variability in the Aitken mode diameter. Their analysis centred around periods of steady state conditions and as a result, may have excluded transient episodes of NPF and favoured air masses in which the aerosol population had undergone substantial cloud processing, leading to relatively invariant Aitken diameters.~~With modal diameters averaging 30 nm, the Aitken aerosol were often smaller than those seen in the continental air masses (Fig. S2) and both their concentration and modal distributions were highly variable, rarely remaining constant for more than a few hours at a time.~~

~~These findings are in good agreement with observations reported by Fossum et al. (2018), from a concurrent cruise in the Atlantic sector of the Southern Ocean, although they observed Aitken aerosol with a slightly larger mode diameter of 42 nm. Likewise, Schmale et al. (2019) reported similar total aerosol number concentrations. The relative change in number concentration between measurements in the mid-latitudes of the Southern Ocean and those taken close to the Antarctic continent during their ACE-SPACE circumnavigation of Antarctica was also similar to our findings.~~

~~An additional smaller Aitken mode centred at approximately 10–20 nm was seen on multiple occasions during these *mSO* periods. It was particularly obvious on 3rd, 6th, 9th and 11th November (Fig. 2) and suggested that NPF had occurred, but that the precursor concentrations or atmospheric conditions had not supported sufficient particle growth to reach diameters comparable to the remainder of the Aitken distribution. The NAIS showed no evidence of aerosol formation or growth of sub-10 nm particles to these sizes, indicating that the NPF events occurred sometime prior to the air mass reaching the ship.~~

~~Episodes of increased Aitken mode number concentrations were most common when air masses maintained a long fetch over the productive region between the Kerguelen Plateau and the Antarctic coastline (Fig. 4(a) and Fig. S1). This was a common occurrence, particularly for *mSO2* and subsequent air masses, and suggests that the Aitken mode observed during these periods is significantly influenced by the biological productivity in that region, leading to NPF from biogenic precursors. However, this characteristic back trajectory path alone does not fully explain the variability in Aitken concentrations and diameters. Specifically, there was no consistent correlation between the Chl-a exposure proxy parameter and any Aitken mode parameter, such as number concentration or mean diameter. Therefore, we have chosen to examine these periods in more detail to identify other contributing influences.~~

4.2.1 *Influences on marine CCN ~~mSO4~~*

$CCN_{0.5\%}$ concentrations were quite similar across the four *mSO* sampling periods, averaging 189 ± 67 cm^{-3}. The accumulation mode number concentrations were strongly correlated with $CCN_{0.5\%}$ (Pearson's correlation coefficient of 0.824, p-value of $< 2.2 \times 10^{-16}$), explaining 68 % of the variability in $CCN_{0.5\%}$ in *mSO* air masses. The remaining variability can be attributed to fluctuations in SSA concentrations or contributions from Aitken mode aerosol with sufficiently large diameter to activate as $CCN_{0.5\%}$. As discussed in Sect. 3.2 and Sect. 3.3, SSA number concentrations could not be adequately constrained and so the observed sea salt mass concentration was used as a proxy. The contribution from Aitken mode aerosol depended on both the aerosol diameter and number concentration. Independently, these two parameters were poorly correlated with $CCN_{0.5\%}$. The correlation was improved by combining them to give the ultrafine aerosol volume (Sect. 3.2), which was weighted towards aerosol sizes that were more likely to be CCN active.

After subtracting the accumulation mode contribution, the remaining $CCN_{0.5\%}$ were strongly correlated with sea salt mass concentrations during *mSO-IV* and, to a lesser extent, during *mSO-III* (Fig. 5). While both *mSO-II* and *mSO-III* shared similar correlation coefficients, the former period exhibited the widest range of non-accumulation mode $CCN_{0.5\%}$ and the narrowest range of sea salt concentrations, and therefore the apparent trend was not physically meaningful.

The strong correlation observed for *mSO-IV* can be attributed to the fact that concurrent $CCN_{0.5\%}$ and sea salt measurements were only available during a brief 15-hour window which coincided with the passage of a cold front across the path of the ship. During the 48 hours prior to reaching the ship, the corresponding air masses experienced median wind speeds of up to 12.6 m s^{-1}, leading to sea salt mass concentrations of up to 0.86 µg m^{-3}. Similarly, a cold front passed the ship shortly before the start of *mSO-III*. During the initial 9 hours of this sampling period, the 48-hour median wind speeds reached as high as 15.6 m s^{-1}, but the maximum observed sea salt mass was 0.62 µg m^{-3}. The discrepancy between these two cases can be

attributed to differences in rainfall history along the air mass trajectories, with 48-hour rainfall totals that were up to an order of magnitude higher in *mSO-III* than *mSO-IV* (Fig. S4).

Comparing the two sampling periods more broadly, the *mSO-III* sampling period occurred at higher latitudes where weather systems are typically more frequent and intense. The mass-based source function predicted much higher sea salt concentrations than were observed throughout *mSO-III* (Fig. S2) due to persistently higher wind speeds, which reached a maximum of 19.4 m s^{-1}. However, only 10 % of the air mass back trajectories for this period remained within the MBL with rainfall rates <0.25 mm h^{-1} during the final 48 hours prior to reaching the ship. By comparison, 83 % of the back trajectories met these requirements for *mSO-IV*, leading to much closer agreement between the modelled and observed concentrations.

Given that the mass-based source function was developed on the basis of steady state SSA concentrations measured during periods of stable wind speeds, it is likely that the unfavourable conditions during *mSO-III* prevented the SSA aerosol from building towards the concentrations predicted by the model. Furthermore, these findings suggest at least two days of historical meteorology should be considered for each sampled air mass when estimating SSA production rates and concentrations over the Southern Ocean.

In contrast to SSA, the ultrafine aerosol volume concentrations were strongly correlated with the non-accumulation mode CCN during most *mSO* sampling periods, with a weaker response during *mSO-III* (Fig. 6). These strong correlations were driven by three episodes of particularly high ultrafine aerosol volume that occurred on 2nd, 6th and 13th February 2015 (Fig. S5a). The associated air mass trajectories were averaged for each episode and altitude profiles were generated to investigate the atmospheric conditions which lead to each event (Fig. S6).

Each case was characterised by relatively low altitude air masses which remained at an average of 240 ± 80 m above sea level, facilitating the uptake of biogenic emissions from the ocean surface. They each spent at least 12 hours above regions of increased biological productivity, indicated by ocean surface Chl-a concentrations well above the regional mean of 0.24 mg m^{-3}, before encountering cold fronts that strongly compressed the boundary layer. The intervening transport times between the biologically active regions and the frontal systems ranged from approximately 48–100 hours, comparable to the estimated lifetime of DMS in the remote MBL (Langley et al., 2010; Barnes et al., 2006). The subsequent strong compression of the MBL likely increased the vapour pressures of DMS oxidation products, leading to increased condensational growth and the observed increases in the Aitken mode diameters.

Of these three episodes, the largest Aitken mode aerosol were observed on 6th February. Due to the passage of the front, the air masses were transported into the free troposphere, returning to the MBL less than 27 hours prior to reaching the ship (Fig. S6d). During this time, rainfall rates peaked at 0.56 mm h^{-1}. As a result, both observations and modelled estimates of sea salt mass concentration were low throughout this episode (Fig. S2), measured at an average of 0.13 ± 0.05 μg m^{-3}. Therefore, assuming minimal contribution to $CCN_{0.5\%}$ from SSA, Aitken mode aerosol contributed up to 181 cm^{-3} or 56% of total $CCN_{0.5\%}$ during this period. For comparison, the highest SSA concentrations were observed on 12th February and were associated with non-accumulation mode CCN concentrations that increased to 77.6 cm^{-3} (Fig. S5b). Due to a coincident increase in ultrafine aerosol volume concentration, it is unclear how much of the increase in $CCN_{0.5\%}$ can be directly attributed to SSA. At most,

SSA may have contributed 34% of the total $CCN_{0.5\%}$. This is consistent with the contribution from SSA at high latitudes as reported in ~~(Quinn et al., 2017)~~Quinn et al. (2017) and supports their finding that nss-SO_4 represent the dominant source of $CCN_{0.5\%}$ even in the remote Southern Ocean.

Air mass trajectories associated with the 6th February enhancement of the Aitken mode showed high sea surface Chl-a concentrations in the vicinity of the Kerguelen Plateau (Fig. S6c). Strong peaks in nucleation mode aerosol concentrations, observed on 3, 7 and 10 February (Fig. 4), also coincided with air mass trajectories that passed over or close to the Kerguelen Plateau (e.g. Fig. S7). However, although they passed over similar concentrations of sea surface Chl-a, they generally did so at almost twice the altitude of the air masses associated with Aitken mode aerosol and likely experienced lower flux rates of biogenic emissions. In addition, they did not encounter such pronounced compression of the MBL in a suitable timeframe after passing the high Chl-a region and were not transported into the free troposphere at any point along the trajectory. As a result, it seems that they developed sufficient concentrations of nss-SO4 precursors to trigger NPF within the MBL, but could not support the same degree of condensational growth into the Aitken diameter range and therefore had negligible impact on CCN concentrations.

~~Shortly after the transition to the *mSO4* sampling period, the N_{10} concentrations peaked at 800 cm^{-3}, due to an abrupt increase in Aitken mode aerosol, with geometric mean diameters that decreased to approximately 22 nm (Fig. S2). As shown in Fig. 4(a), the initial hours of *mSO4* were also associated with a sudden increase in the Chl-a exposure proxy parameter, indicative of the amount of time that the air masses spent within the MBL over the Kerguelen-Antarctic productive region and the corresponding Chl-a concentration along their trajectories. As such, the air masses may have been exposed to an increased flux of biogenic precursors. Furthermore, the trajectories exhibited a short excursion into the free troposphere that could have triggered NPF, resulting in the smaller aerosol mode initially observed during *mSO4*.~~

~~After approximately 14 hours, the Aitken number concentrations briefly dropped to the same level as the accumulation mode aerosol despite Chl-a exposures higher than at any other point during the voyage. SSA mass concentrations demonstrated a strong peak during this time (Fig. S3) and there was a general decrease in the altitude of the back trajectories, with less time spent in the free troposphere. Together these observations likely explain the diminished Aitken mode, with weakened vertical transport inhibiting secondary aerosol formation and depletion of condensable material due to the high surface area presented by SSA.~~

~~The Aitken mode then returned to even higher concentrations than observed at the start of the *mSO4* period despite back trajectories remaining within the MBL. Both SSA mass concentrations and accumulation mode number concentrations rapidly decreased, while total rainfall progressively increased along the air mass trajectories (Fig. S4), suggesting that these condensation sinks must have been sufficiently depleted to permit NPF to occur within the MBL.~~

~~4.2.2 *mSO3*~~

~~A strong increase in Aitken number concentrations was also observed midway through the *mSO3* sampling period (Fig. 4(b)). This coincided with air mass trajectories with a long fetch over the productive region, followed by a brief excursion into the~~

free troposphere as they passed through a cold front associated with a strong low-pressure system. As seen for air masses early in *mSO4*, the assumed increased flux of precursors followed by vertical transport likely provided the necessary conditions for substantial Aitken mode production. It should be noted that the initial 16 hours of *mSO3* exhibited much higher Chl-a exposures and similar levels of vertical transport, however there was much less impact on the Aitken mode. Again, SSA concentrations were particularly high during these initial hours (Fig. S3) and may have provided a greater condensation sink inhibiting NPF and growth into the Aitken mode.

4.2.3 *mSO2*

The *mSO2* air mass exhibited an initial burst of Aitken mode aerosol with a mean diameter of 20 nm. This was similarly associated with a strong frontal system which drove the air mass into the free troposphere and was accompanied by increased rainfall, leading to depletion of the accumulation mode. The vertical transport and subsequent entrainment into the MBL occurred approximately 12 hours prior to the air mass reaching the ship, allowing minimal mixing or dilution time within the MBL and leading to the intense and well-defined mode displayed in Fig. 2. Similar conditions persisted for most of the day, with trajectories over the same approximate regions and vertical transport close to the ship, however the rainfall somewhat decreased. Within three hours, the accumulation mode returned, and the 20 nm mode was almost entirely replaced by an Aitken mode with the largest mean diameters seen throughout the voyage. The large Aitken mode diameters could be due to the transition to an aged air mass which had time for growth via coagulation and/or from condensation onto an existing Aitken population, significantly increasing its size. Subsequently, rainfall rates almost doubled, once again leading to depletion of both the accumulation mode and the larger Aitken mode diameters.

Each of these three *mSO* periods presents evidence of the apparent role of synoptic scale weather systems in promoting NPF and growth of the Aitken mode by providing convective transport into the free troposphere and depletion of competing condensation sinks through rainfall. However, the high wind speeds associated with these weather systems can also lead to SSA production. During *mSO3* and *mSO4*, high SSA concentrations seem to have increased the condensation sink and inhibited NPF. In contrast, SSA concentrations did not substantially increase during mSO2 despite back trajectories which passed through a cold front. Other studies have discussed significant uncertainties in modelling the SSA flux, with dependence on water temperature, biological activity and other parameters (Saliba et al., 2019; Grythe et al., 2014). The apparent impact of SSA on precursor availability for NPF and secondary nss SO4 formation highlights the importance of improving this SSA flux parameterisation.

4.3 Continental and coastal Australian air masses (*cAU*)

The cAU air masses were encountered as the ship moved southward between 54.2 °S and 58.5 °S. During this time, ~~T~~the back trajectories indicated air masses circulating around a persistent high-pressure system which was centred approximately 1000 km south of the Australian mainland (Fig. 8~~6~~). Radon, BC and organic aerosol concentrations initially rose above the

marine background level (Fig. 2~~(b)~~ and Fig. S3~~8~~), peaking at hourly means of 220 mBq m^{-3}, 0.027 μg m^{-3} and 0.18 μg m^{-3}, respectively. The interpretation of this elevated radon concentration has been discussed in detail by ~~Chambers et al. (2018)~~ Chambers et al. (2018)and it suggests that the air mass was influenced by terrestrial emissions. However given that the radon concentrations were approximately an order of magnitude lower than is commonly seen over major land masses (Chambers et al., 2011) and the trajectories spent approximately 54% of their 7-day duration in the free troposphere (Fig. S9), they likely represented long range transport of aged and diluted terrestrial emissions.

N_{10} concentrations were approximately halved compared to the *mSO* air masses, including almost complete loss of the nucleation mode. However the accumulation mode concentrations increased to dominate the size distribution (Fig. 7) and both the Aitken and accumulation modes exhibited the largest mean diameters of the voyage (Table 1 and Fig. S3). Overall, the net result was a slight increase in $CCN_{0.5\%}$ relative to the *mSO* air masses, with a median concentration of 200 cm^{-3}. ~~As the ship moved southward of 54.2° S, the aerosol size distribution became dominated by the accumulation mode (Fig. 5), while both aerosol modes exhibited the largest mean diameters of the voyage and N_{10} concentrations remained persistently low (Table 1 and Fig. S2). Radon, BC and organic aerosol concentrations initially rose above the marine background level (Fig. 2(b) and Fig. S3), peaking at hourly means of 220 mBq m^{-3}, 0.027 μg m^{-3} and 0.18 μg m^{-3}, respectively. The interpretation of this elevated radon concentration has been discussed in detail by Chambers et al. (2018) and it suggests that the air mass was influenced by terrestrial emissions. The back trajectories indicated air masses circulating around a persistent high pressure system which was centred approximately 1000 km south of the Australian mainland (Fig. 6). Within the 7 day extent of each back trajectory, there was little to no passage over the Australian continent itself, however continental species could have persisted from prior passage over the continent because the air masses measured during this period were in the free troposphere for greater than 50% of the time. As a result of this bias towards large diameters, and despite the relatively high organic loading, 79 % of the total aerosol number activated as $CCN_{0.5\%}$. This high activation ratio was particularly demonstrated during the afternoon and evening of 4th February, when rainfall in the vicinity of the ship heavily depleted the aerosol load, with total number concentrations as low as 63.9 cm^{-3}.~~

~~Over the following day (5 February 2015), as the ship moved further southwards from the Australian continent, radon and BC concentrations diminished to near background levels (60 mBq m^{-3} and 9 ng m^{-3}, respectively). However, other observations did not reflect a return to the usual maritime sampling conditions. There was little variation to the aerosol size distribution and back trajectory paths. Organic aerosol concentrations progressively fell below the detection limit, but SSA also remained low. MSA and non-MSA sulfates rose to peak hourly-average concentrations of 0.035 ug m^{-3} and 0.316 ug m^{-3}, the highest values for the voyage and the $CCN_{0.5\%}$ activation ratio reached a campaign maximum of 93 %. As shown in Fig. 1, a wide band of elevated biological activity was present in the waters south of the Australian coastline. The high pressure synoptic system had persisted in this region for at least 5 days prior to the air masses reaching the ship, deflecting cold fronts and their associated high wind speeds and rainfall. High biological activity, a relatively low SSA condensation sink and potential for cloud processing created conditions for the growth of large accumulation mode nss SO_4, rather than conditions promoting the high concentrations of Aitken mode aerosol typically observed from the *mSO* air masses.~~

4.4 Continental Antarctic air masses (*cAA*)

~~Each *cAA* period was preceded by strong low pressure systems centred at approximately 60° S and advancing eastwards towards the ship. As these low pressure systems advanced, the back trajectories diverted southwards, bringing air masses from the Antarctic continent (Fig. 7 and Fig. 8). The first of these periods (*cAA1*) was~~The *cAA* air masses were encountered when the ship was within 400 km of the Antarctic coastline, ~~while the ship was located~~ between the latitudes of 64–65.1° S, and during the northward transit between the latitudes of 57.5–60.1° S, at approximately 1000 km from the Antarctic coast. Each *cAA* period was preceded by strong low-pressure systems centred at approximately 60° S, which diverted the air masses northwards from over the Antarctic continent and towards the ship. (Fig. 9 and Fig. 10). While over the continent, the air masses were almost constantly within the free troposphere (Fig. S10), typically dropping into the MBL after leaving the coastal region, as per ~~similar to what was~~ the dominant trajectory regime observed in East Antarctica during the austral spring of 2012 ~~(Humphries et al., 2016)~~(Humphries et al., 2016).

The continental influence on the *cAA-I* air masses was supported by mean radon concentrations of 82 ± 25 mBq m^{-3}~~,~~. This was consistent with the increase in summer-autumn radon concentrations at latitudes above 64° S, as reported by Chambers et al. (2018), through a combination of increased coastal emissions (due to exposed rocks and soils) and subsidence of terrestrially-influenced tropospheric air over Antarctica. ~~The measurements from approximately half of this 37 hour period were affected by ship exhaust and have been excluded. In the remaining measurements, BC mostly remained at levels comparable to the *mSO* periods, with the exception of the final four hours during which time BC briefly peaked at 0.024 ug m^{-3}. As indicated by low N_{10} concentrations and favourable wind conditions, these latter hours of sampling were not characteristic of direct ship emissions, suggesting that the elevated BC may have been from Antarctic terrestrial sources or residual ship exhaust emitted during the southward leg of the voyage. Alternatively, Chambers et al. (2017) found evidence for air masses influenced by mid to low latitude land masses which were transported through the free troposphere, subsided over Antarctica and were subsequently exported to the MBL via katabatic outflows. As such, the radon and BC concentrations observed during *cAA1* may include residual continental emissions from Australia or New Zealand, present in air masses which subsided over the Antarctic continent.~~

As with the *cAU* air mass, the majority of aerosol~~N_{10} concentrations~~ were ~~well below the voyage mean and~~in the accumulation mode ~~represented 70 % of the total number concentration~~ (Fig. ~~9~~11, Table S1), in close agreement with *cAA* observations given by ~~(Fossum et al., 2018)~~Fossum et al. (2018). For *cAA-I*, this led to median $CCN_{0.5\%}$ concentrations that were 25% higher than any other air mass, at 252 cm^{-3}.

The transitions between the *mSO* and *cAA-II* air masses were more gradual, with a greater proportion of the back trajectories passing over the coastal region (Fig. 8). In addition, the increased distance to the ship lead to more dilution and mixing within the MBL, resulting in radon concentrations that were only slightly elevated above the marine background, at a mean of 62.5 mBq m^{-3}. Nonetheless, the period shared very similar N_{10} concentrations, nss-SO_4 mass concentrations and a dominant accumulation mode as *cAA-I* (Table S1, Fig. S3 and Fig. S8).

~~The additional small mode seen at approximately 10 nm in Fig. 9 can be attributed to a brief period during *cAA2* in which a tri-modal distribution was observed and will be discussed in further detail below.~~

~~During *cAA1*, the large contribution from the accumulation mode drove $CCN_{0.5\%}$ concentrations to their highest level with a mean of 240 cm^{-3} and a $CCN_{0.5\%}$ activation ratio of 0.79.~~ The transitions between *mSO* and *cAA~~ 1~~ I* air masses were well defined during both the southward and northward transits, with pronounced and persistent changes particularly in N_{10} and Aitken number concentrations, as well as meteorological parameters such as air temperature and absolute humidity (Fig. ~~S5~~S11). They occurred across a latitude range of approximately 64.0–64.5° S. During a nearby cruise in the early austral spring of 2012 and in the same region, Humphries et al. (2016) observed a similar abrupt transition at 64.4° S and attributed this to a shift between the Ferrel atmospheric cell and the polar cell. It is interesting to note that while they reported comparable N_{10} concentrations in the polar region, these decreased to a mean of 194 cm^{-3} at lower latitudes, rather than increasing as was seen during the ~~Cold Water Trial~~CWT voyage reported on here. This may reflect greater seasonal variability in the Southern Ocean compared to polar waters, with lower oceanic productivity in the early spring leading to reduced rates of aerosol formation and growth to diameters above 10 nm. Nonetheless it is difficult to draw conclusions from these two datasets in isolation, highlighting the need for further latitudinal and seasonal studies in this region.

~~The *cAA1* period was also characterised by the lowest mass concentrations of SSA and as a result, nss-SO_4 represented 72.5 % of the sub-micron aerosol composition. Particularly at 40 and 150 nm, the aerosol exhibited less volatility than almost any other time during the voyage, suggesting minimal contribution from sulfuric acid. Given the presence of seal and penguin colonies on the Antarctic coastline, the low volatility may reflect the neutralising effect of these biogenic sources of nitrogen to air masses passing over the coastline (Legrand et al., 1998), transforming sulfuric acid into ammonium sulfate and bisulfate. Again, these aerosol properties were generally consistent with the concurrent measurements of *cAA* air masses off the coast of West Antarctica, given by Fossum et al. (2018). The only significant exception was the contribution from MSA which could not be adequately quantified at such low aerosol concentrations due to the previously discussed instrument limitations. Regardless, since *cAA1* air masses persistently maintained high altitudes while over the landmass, the similarity between observations on opposite sides of the continent may reflect a degree of uniformity in the aerosol populations throughout the Antarctic free troposphere at this time of year.~~

~~The second period of *cAA* air masses (*cAA2*) was observed over a 17 hour period while the ship was between 57.5–60.1° S, approximately 1000 km from the Antarctic coast. Compared to *cAA1*, the back trajectories spent less time in the free troposphere, except during the first few hours when a cold front passed through the region. The transitions between the *mSO* and *cAA2* air masses were more gradual, with a greater proportion of each back trajectory passing over the coastal region (Fig. 8), particularly during the four hours at the start and end of this period. Radon concentrations were only slightly elevated above the marine background, at a mean of 62.5 mBq m^{-3}, but the period otherwise shared the same mean N_{10} concentration and nss-SO_4 mass concentration as *cAA1* (Table S1, Fig. S2 and Fig. S3).~~

~~The accumulation mode retained a similar mean diameter to *cAA1* at 122 nm, however its contribution to the total size distribution decreased to 44 %. In addition, a distinct tri-modal distribution developed during the first six hours of *cAA2*, with~~

an additional small Aitken mode centred at approximately 15 nm (Fig. 2). The corresponding back trajectories spent increased time over the highly productive coastal region, which may have offered more opportunities for uptake of biogenic sulfate precursors. Likewise, the passing weather system may have provided sufficient uplift to spur NPF. If so, it seems that the meteorological conditions or precursor concentrations were insufficient to support further growth into the Aitken size range commonly seen in the *cAA* air masses.

Another marked difference between the two *cAA* periods can be seen in the elevated SSA mass concentrations during *cAA2*. As highlighted above, both high SSA concentrations and the presence of small diameter Aitken mode aerosol were characteristic of the *mSO* sampling periods. Given the relatively low radon concentrations during *cAA2*, substantial dilution and mixing likely occurred over the longer transport range. Therefore, these two *cAA* periods may demonstrate the progressive transition of air masses from being strongly influenced by continental outflow into characteristic maritime air masses as they are transported further from the continent.

4.5 Latitudinal trends

The north-south track from coastal Australian to polar Antarctic waters provided an ideal opportunity to examine trends in aerosol properties across the latitudinal range of the Southern Ocean (Fig. S6 and Fig. S7). Simple linear regression with respect to latitude indicated an approximate 25% decrease in the mean diameter of the Aitken mode between 46–63° S, however the accumulation mode did not exhibit a significant trend. In contrast, the hygroscopicity of 150 nm aerosol increased from 0.40 to 0.59 between 51–63° S, while there was no significant change at 40 nm. The increased density of intense weather systems at high latitudes would have increased scavenging rates for accumulation mode aerosol while promoting an increased SSA population. In turn, this likely lead to the reduction in aerosol diameter and an SSA-driven increase in hygroscopicity at larger diameters without substantially affecting the 40 nm population.

As previously discussed, N_{10}, Aitken, accumulation and CCN number concentrations changed substantially within the polar cell, south of 64° S. With the exception of this region, and despite the above trends in diameter and hygroscopicity, the concentrations did not exhibit any clear latitudinal dependence over the breadth of the Southern Ocean (Fig. S8 and Fig. S9). Instead they showed high levels of variability, particularly south of 48° S, driven by short term changes in air mass and the impact of synoptic events on aerosol production and scavenging rates. For example, at 55° S, there was a pronounced decrease in both CCN and N_{10} concentrations. Although this occurred in both the southward and northward transits, it is unlikely to be a consistent latitudinal feature since it can be attributed to transient events including aerosol losses during the *cAU* rain event and the brief episode of high SSA mass concentrations coinciding with Aitken mode depletion during *mSO4*.

5 Conclusions

We have presented the first comprehensive study of aerosol properties targeting the full latitudinal width of the Southern Ocean south of Australia. The voyage was carried out during the austral summer and extended to the edge of the marginal ice zone at 65° S. Despite the short 2-week timeframe of this study, synoptic scale weather systems interrupted the usual *mSO* air masses on three occasions, drawing continental-influenced air masses from Australia and Antarctica over 1000 km into the Southern Ocean. In line with observations by Humphries et al. (2016), a pronounced change in aerosol number concentrations, size distributions, CCN activity, air mass trajectories and other meteorological parameters offer support for a transition into the polar atmospheric cell at an approximate latitude of 64° S.

During *cAA-I*, increased accumulation mode aerosol in the continental outflow led to 25 % higher CCN concentrations than the voyage mean. All other air masses exhibited similar median $CCN_{0.5\%}$ concentrations, but with substantially higher variability in the *mSO* air masses. Increases in SSA were directly linked to this variability for only two 10-hour episodes during the northward transit. In part, this was attributed to the competing influence of strong secondary aerosol production caused by high levels of summer-time marine productivity. However, the frequent synoptic-level weather systems in the Southern Ocean are typically accompanied by rainfall and convective transport into the free troposphere. We suggest that SSA rarely reach their wind speed-dependent equilibrium concentration unless the air mass remains within the MBL and is not exposed to substantial rainfall (e.g. >0.25 mm h^{-1}) for approximately 48 hours.

During this voyage, secondary aerosol production and growth of the Aitken mode diameter had a stronger influence than SSA, leading to non-accumulation mode CCN concentrations that were up to 200 % higher than the corresponding peaks seen during SSA-influenced episodes. However, although there were several regions of high biological productivity in this sector of the Southern Ocean, Aitken mode aerosol only exhibited growth to CCN-relevant diameters in three instances. These periods were marked by low air mass trajectory altitudes, several hours of exposure to a region of high biological activity, sufficient time for gas phase photochemistry to occur and finally strong compression of the MBL during the passage of a cold front which promoted NPF or aerosol condensational growth. In the absence of a cold front, or when it coincided with a biologically productive region, high concentrations of nucleation mode aerosol were formed with minimal impact on CCN.

The wind-mediated SSA model predicted the highest concentrations of SSA at high latitudes where cyclonic conditions were most frequent. However, the impact of these weather systems on air mass altitudes and aerosol wet scavenging rates significantly limited the observed SSA concentrations and in fact the highest concentrations were observed during stable weather conditions, more commonly seen at lower latitudes. Clearly, air mass meteorological history must be carefully considered when predicting SSA concentrations.

These results highlight the fundamental role of synoptic-level weather systems in promoting or inhibiting SSA and CCN-relevant secondary aerosol. Given the current scarcity of data from the Southern Ocean, and the over-representation of summer-time voyages, there is a clear need for a greater body of data. This would allow examination of whether the aerosol population

exhibits such variability during other seasons and therefore its dependence on biological activity. It would also be valuable to assess the frequency, duration and characteristics of the long-range transport events.

~~Heightened summer-time marine productivity was clearly apparent with strong Chl-a concentrations along the Antarctic coastline and extending from the Kerguelen Plateau towards Antarctica. On multiple occasions, the Aitken mode number fraction increased to 75 % of the total aerosol population in air masses passing over the Kerguelen–Antarctic productive region. However, this was typically associated with relatively small Aitken mode geometric mean diameters, at approximately 30 nm. As a result, the number concentration of Aitken mode aerosol correlated poorly with CCN concentrations throughout most of the voyage. Assuming that this is a true reflection of typical aerosol populations in this region of the Southern Ocean, it suggests that nss-SO_4 NPF from this region do not have a direct impact on the local cloud droplet number concentration and that further cloud processing or nss-SO_4 condensation is required to grow them to cloud-active diameters.~~

~~CCN concentrations were more significantly impacted by changes in air mass, with much higher CCN ratios observed in aerosol transported from the Antarctic and Australian continents. These episodes were observed at distances of over 1000 km from either continent, demonstrating that long range transport of continental air masses can effectively influence the full width of the Southern Ocean, as previously proposed by Chambers et al. (2018). Furthermore, it is interesting to note that two episodes were observed during this 15-day dataset, which suggests that there could be an important contribution to the Southern Ocean from aerosol transported from the Antarctic and Australian continents.~~

~~The changes in air mass were driven by synoptic-scale weather systems. The prolonged transport of continental and coastal Australian aerosol was maintained by a persistent, slow-moving high pressure system. Similarly, during the *cAA2* period, a series of low-pressure systems drew the Antarctic air masses deep into the Southern Ocean. During *mSO3* and *mSO4*, increased generation of SSA inhibited the formation and growth of the Aitken mode, while in *mSO2*, heavy rainfall and depletion of larger-diameter particles was associated with an intense burst of Aitken mode aerosol. Finally, aside for the latter part of *mSO4*, enhancement of the Aitken population was consistently associated with vertical transport between the MBL and the free troposphere during the passage of cold fronts. Clearly, synoptic systems play a fundamental role in mediating aerosol properties in the Southern Ocean through their impact on air mass origins and trajectories, SSA production, aerosol removal rates due to rainfall and vertical transport between the MBL and the free troposphere.~~

~~In line with observations by Humphries et al. (2016), a pronounced change in aerosol number concentrations, size distributions, CCN activity, air mass trajectories and other meteorological parameters offer support for a transition into the polar atmospheric cell at an approximate latitude of 64° S. The highest CCN concentrations were observed within this region, despite low N_{10} concentrations, with air masses primarily sourced from the free troposphere over the Antarctic continent. In contrast, most aerosol properties exhibited little dependence on latitude throughout the remainder of the voyage. Instead, austral summer influences from marine productivity, long range transport, and synoptic weather systems resulted in a high degree of variability which outweighed most latitudinal trends.~~

~~Given the current scarcity of data from the Southern Ocean, and the over-representation of summer-time voyages, there is a clear need for a greater body of data. This would allow examination of whether the aerosol population exhibits such variability~~

~~during other seasons and therefore its dependence on biological activity. It would also be valuable to assess the frequency, duration and characteristics of the long-range transport events.~~

6 Data availability

The underlying research data can be accessed upon request to the corresponding author (Zoran Ristovski; z.ristovski@qut.edu.au).

7 Author contribution

ZDR was chief scientist for the Cold Water Trial campaign and coordinated the investigation in conjunction with MDK. ZDR, LTC and JA managed data collection, daily maintenance and calibration of the aerosol instrumentation throughout the voyage. Installation, calibration and data analysis for the ACSM was performed by PS. Processing and interpretation of Radon-222 data was completed by SDC and AGW. All other data analysis and interpretation was led by JA with input from all authors, particularly LTC and ZDR. JA led manuscript preparation with input from all authors.

8 Acknowledgements

This work was funded by an Australian Government Research Training Program Scholarship and an ARC Discovery grant (DP150101649). We acknowledge the NASA Goddard Space Flight Centre, Ocean Biology Processing Group for the provision of the MODIS Aqua chlorophyll data and the NOAA Air Resources Laboratory (ARL) for the provision and support for the HYSPLIT transport and dispersion model. The Authors wish to thank the CSIRO Marine National Facility (MNF) for its support in the form of sea time on RV Investigator, support personnel, scientific equipment and data management. In particular, we thank the technical and IT support personnel on board the voyage, including Ian McRobert, William Ponsonby, Brett Muir, Steve Thomas, Hugh Barker, Stewart Wilde and Anoosh Sarraf. We gratefully acknowledge Jason Ward and James Harnwell (CSIRO) for their ongoing support of the permanent aerosol instrumentation on board. All data and samples acquired on the voyage are made publically available in accordance with MNF Policy from the CSIRO Data Access Portal (https://data.csiro.au/dap/).

References

Albrecht, B. A.: Aerosols, Cloud Microphysics, and Fractional Cloudiness, Science, 245, 1227-1230, doi: 10.1126/science.245.4923.1227, 1989.

Andreae, M. O., and Rosenfeld, D.: Aerosol–cloud–precipitation interactions. Part 1. The nature and sources of cloud-active aerosols, Earth-Sci. Rev., 89, 13-41, doi: 10.1016/j.earscirev.2008.03.001, 2008.

Ault, A. P., Moffet, R. C., Baltrusaitis, J., Collins, D. B., Ruppel, M. J., Cuadra-Rodriguez, L. A., Zhao, D., Guasco, T. L., Ebben, C. J., Geiger, F. M., Bertram, T. H., Prather, K. A., and Grassian, V. H.: Size-Dependent Changes in Sea Spray Aerosol Composition and Properties with Different Seawater Conditions, Environ. Sci. Technol., 47, 5603-5612, doi: 10.1021/es400416g, 2013.

Barnes, I., Hjorth, J., and Mihalopoulos, N.: Dimethyl Sulfide and Dimethyl Sulfoxide and Their Oxidation in the Atmosphere, Chemical Reviews, 106, 940-975, doi: 10.1021/cr020529+, 2006.

Bates, T. S., Kapustin, V. N., Quinn, P. K., Covert, D. S., Coffman, D. J., Mari, C., Durkee, P. A., De Bruyn, W. J., and Saltzman, E. S.: Processes controlling the distribution of aerosol particles in the lower marine boundary layer during the First Aerosol Characterization Experiment (ACE 1), 103, 16369-16383, doi: 10.1029/97jd03720, 1998.

Bianchi, F., Tröstl, J., Junninen, H., Frege, C., Henne, S., Hoyle, C. R., Molteni, U., Herrmann, E., Adamov, A., Bukowiecki, N., Chen, X., Duplissy, J., Gysel, M., Hutterli, M., Kangasluoma, J., Kontkanen, J., Kürten, A., Manninen, H. E., Münch, S., Peräkylä, O., Petäjä, T., Rondo, L., Williamson, C., Weingartner, E., Curtius, J., Worsnop, D. R., Kulmala, M., Dommen, J., and Baltensperger, U.: New particle formation in the free troposphere: A question of chemistry and timing, Science, 352, 1109-1112, doi: 10.1126/science.aad5456, 2016.

Callaghan, A., de Leeuw, G., Cohen, L., and O'Dowd, C. D.: Relationship of oceanic whitecap coverage to wind speed and wind history, Geophys. Res. Lett., 35, doi: 10.1029/2008gl036165, 2008.

Chambers, S., Williams, A. G., Zahorowski, W., Griffiths, A., and Crawford, J.: Separating remote fetch and local mixing influences on vertical radon measurements in the lower atmosphere, Tellus B, 63, 843-859, doi: 10.1111/j.1600-0889.2011.00565.x, 2011.

Chambers, S. D., Preunkert, S., Weller, R., Hong, S.-B., Humphries, R. S., Tositti, L., Angot, H., Legrand, M., Williams, A. G., Griffiths, A. D., Crawford, J., Simmons, J., Choi, T. J., Krummel, P. B., Molloy, S., Loh, Z., Galbally, I., Wilson, S., Magand, O., Sprovieri, F., Pirrone, N., and Dommergue, A.: Characterizing Atmospheric Transport Pathways to Antarctica and the Remote Southern Ocean Using Radon-222, Front. Earth Sci., 6, doi: 10.3389/feart.2018.00190, 2018.

Clarke, A. D., Varner, J. L., Eisele, F., Mauldin, R. L., Tanner, D., and Litchy, M.: Particle production in the remote marine atmosphere: Cloud outflow and subsidence during ACE 1, J. Geophys. Res.-Atmos., 103, 16397-16409, doi: 10.1029/97jd02987, 1998.

Covert, D. S., Kapustin, V. N., Bates, T. S., and Quinn, P. K.: Physical properties of marine boundary layer aerosol particles of the mid-Pacific in relation to sources and meteorological transport, 101, 6919-6930, doi: 10.1029/95jd03068, 1996.

Cravigan, L. T., Ristovski, Z., Modini, R. L., Keywood, M. D., and Gras, J. L.: Observation of sea-salt fraction in sub-100 nm diameter particles at Cape Grim, J. Geophys. Res.-Atmos., 120, 1848-1864, doi: 10.1002/2014JD022601, 2015.

Cravigan, L. T., Mallet, M. D., Vaattovaara, P., Harvey, M. J., Law, C. S., Modini, R. L., Russell, L. M., Stelcer, E., Cohen, D. D., Olsen, G., Safi, K., Burrell, T. J., and Ristovski, Z.: Sea spray aerosol organic enrichment, water uptake and surface tension effects, Atmos. Chem. Phys. Discuss., 2019, 1-35, doi: 10.5194/acp-2019-797, 2019.

Dall'Osto, M., Ovadnevaite, J., Paglione, M., Beddows, D. C. S., Ceburnis, D., Cree, C., Cortés, P., Zamanillo, M., Nunes, S. O., Pérez, G. L., Ortega-Retuerta, E., Emelianov, M., Vaqué, D., Marrasé, C., Estrada, M., Sala, M. M., Vidal, M., Fitzsimons, M. F., Beale, R., Airs, R., Rinaldi, M., Decesari, S., Cristina Facchini, M., Harrison, R. M., O'Dowd, C., and Simó, R.: Antarctic sea ice region as a source of biogenic organic nitrogen in aerosols, Sci. Rep.-UK, 7, 6047, doi: 10.1038/s41598-017-06188-x, 2017.

Draxler, R. R.: Evaluation of an Ensemble Dispersion Calculation, J. Appl. Meteorol., 42, 308-317, doi: 10.1175/1520-0450(2003)042<0308:eoaedc>2.0.co;2, 2003.

Dusek, U., Frank, G. P., Hildebrandt, L., Curtius, J., Schneider, J., Walter, S., Chand, D., Drewnick, F., Hings, S., Jung, D., Borrmann, S., and Andreae, M. O.: Size matters more than chemistry for cloud-nucleating ability of aerosol particles, Science, 312, 1375-1378, doi: 10.1126/science.1125261, 2006.

Fossum, K. N., Ovadnevaite, J., Ceburnis, D., Dall'Osto, M., Marullo, S., Bellacicco, M., Simó, R., Liu, D., Flynn, M., Zuend, A., and O'Dowd, C.: Summertime Primary and Secondary Contributions to Southern Ocean Cloud Condensation Nuclei, Sci. Rep.-UK, 8, 13844, doi: 10.1038/s41598-018-32047-4, 2018.

Fröhlich, R., Cubison, M. J., Slowik, J. G., Bukowiecki, N., Prévôt, A. S. H., Baltensperger, U., Schneider, J., Kimmel, J. R., Gonin, M., Rohner, U., Worsnop, D. R., and Jayne, J. T.: The ToF-ACSM: a portable aerosol chemical speciation monitor with TOFMS detection, Atmos. Meas. Tech., 6, 3225-3241, doi: 10.5194/amt-6-3225-2013, 2013.

GLOBALVIEW-CO: Co-operative Atmospheric Data Integration Project - Carbon Monoxide, CD-ROM, NOAA ESRL, Boulder, Colorado, USA, [Also available on Internet via anonymous FTP to aftp.cmdl.noaa.gov, Path: products/globalview/co], 2009.

Haywood, J., and Boucher, O.: Estimates of the direct and indirect radiative forcing due to tropospheric aerosols: A review, Rev. Geophys., 38, 513-543, doi: 10.1029/1999RG000078, 2000.

Humphries, R. S., Klekociuk, A. R., Schofield, R., Keywood, M., Ward, J., and Wilson, S. R.: Unexpectedly high ultrafine aerosol concentrations above East Antarctic sea ice, Atmos. Chem. Phys., 16, 2185-2206, doi: 10.5194/acp-16-2185-2016, 2016.

Humphries, R. S., McRobert, I. M., Ponsonby, W. A., Ward, J. P., Keywood, M. D., Loh, Z. M., Krummel, P. B., and Harnwell, J.: Identification of platform exhaust on the RV Investigator, Atmos. Meas. Tech., 12, 3019-3038, doi: 10.5194/amt-12-3019-2019, 2019.
Jayne, J. T., Leard, D. C., Zhang, X., Davidovits, P., Smith, K. A., Kolb, C. E., and Worsnop, D. R.: Development of an Aerosol Mass Spectrometer for Size and Composition Analysis of Submicron Particles, Aerosol Sci. Technol., 33, 49-70, doi: 10.1080/027868200410840, 2000.
Kim, J., Yoon, Y. J., Gim, Y., Kang, H. J., Choi, J. H., Park, K. T., and Lee, B. Y.: Seasonal variations in physical characteristics of aerosol particles at the King Sejong Station, Antarctic Peninsula, Atmos. Chem. Phys., 17, 12985-12999, doi: 10.5194/acp-17-12985-2017, 2017.
Langley, L., Leaitch, W. R., Lohmann, U., Shantz, N. C., and Worsnop, D. R.: Contributions from DMS and ship emissions to CCN observed over the summertime North Pacific, Atmos. Chem. Phys., 10, 1287-1314, doi: 10.5194/acp-10-1287-2010, 2010.
Lewis, E. R., Lewis, R., and Schwartz, S. E.: Sea salt aerosol production: mechanisms, methods, measurements, and models, American Geophysical Union, 2004.
Lin, G., Qian, Y., Yan, H., Zhao, C., Ghan, S. J., Easter, R., and Zhang, K.: Quantification of marine aerosol subgrid variability and its correlation with clouds based on high-resolution regional modeling, J. Geophys. Res.-Atmos., 122, 6329-6346, doi: 10.1002/2017jd026567, 2017.
Liu, P. S. K., Deng, R., Smith, K. A., Williams, L. R., Jayne, J. T., Canagaratna, M. R., Moore, K., Onasch, T. B., Worsnop, D. R., and Deshler, T.: Transmission Efficiency of an Aerodynamic Focusing Lens System: Comparison of Model Calculations and Laboratory Measurements for the Aerodyne Aerosol Mass Spectrometer, Aerosol Sci. Technol., 41, 721-733, doi: 10.1080/02786820701422278, 2007.
Modini, R. L., Frossard, A. A., Ahlm, L., Russell, L. M., Corrigan, C. E., Roberts, G. C., Hawkins, L. N., Schroder, J. C., Bertram, A. K., Zhao, R., Lee, A. K. Y., Abbatt, J. P. D., Lin, J., Nenes, A., Wang, Z., Wonaschütz, A., Sorooshian, A., Noone, K. J., Jonsson, H., Seinfeld, J. H., Toom-Sauntry, D., Macdonald, A. M., and Leaitch, W. R.: Primary marine aerosol-cloud interactions off the coast of California, J. Geophys. Res.-Atmos., 120, 4282-4303, doi: 10.1002/2014jd022963, 2015.
Myhre, G., Shindell, D., Bréon, F.-M., Collins, W., Fuglestvedt, J., Huang, J., Koch, D., Lamarque, J.-F., Lee, D., Mendoza, B., Nakajima, T., Robock, A., Stephens, G., Takemura, T., and Zhang, H.: Anthropogenic and Natural Radiative Forcing, in: Climate Change 2013: The Physical Science Basis. Contribution of Working Group I to the Fifth Assessment Report of the Intergovernmental Panel on Climate Change, edited by: Stocker, T. F., Qin, D., Plattner, G.-K., Tignor, M., Allen, S. K., Boschung, J., Nauels, A., Xia, Y., Bex, V., and Midgley, P. M., Cambridge University Press, Cambridge, United Kingdom and New York, NY, USA, 2013.
O'Dowd, C. D., and de Leeuw, G.: Marine aerosol production: a review of the current knowledge, Philos. T. R. Soc. A, 365, 1753, 2007.
O'Shea, S. J., Choularton, T. W., Flynn, M., Bower, K. N., Gallagher, M., Crosier, J., Williams, P., Crawford, I., Fleming, Z. L., Listowski, C., Kirchgaessner, A., Ladkin, R. S., and Lachlan-Cope, T.: In situ measurements of cloud microphysics and aerosol over coastal Antarctica during the MAC campaign, Atmos. Chem. Phys., 17, 13049-13070, doi: 10.5194/acp-17-13049-2017, 2017.
OBPG: Moderate-resolution Imaging Spectroradiometer (MODIS) Aqua Chlorophyll Data, NASA OB.DAAC, Greenbelt, MD, USA, 2018.
Ovadnevaite, J., Ceburnis, D., Canagaratna, M., Berresheim, H., Bialek, J., Martucci, G., Worsnop, D. R., and O'Dowd, C.: On the effect of wind speed on submicron sea salt mass concentrations and source fluxes, J. Geophys. Res.-Atmos., 117, doi: 10.1029/2011jd017379, 2012.
Protat, A., Schulz, E., Rikus, L., Sun, Z., Xiao, Y., and Keywood, M.: Shipborne observations of the radiative effect of Southern Ocean clouds, J. Geophys. Res.-Atmos., 122, 318-328, doi: 10.1002/2016jd026061, 2017.
Quinn, P. K., Coffman, D. J., Johnson, J. E., Upchurch, L. M., and Bates, T. S.: Small fraction of marine cloud condensation nuclei made up of sea spray aerosol, Nat. Geosci., 10, 674-679, doi: 10.1038/ngeo3003, 2017.
Rosenfeld, D., Zhu, Y., Wang, M., Zheng, Y., Goren, T., and Yu, S.: Aerosol-driven droplet concentrations dominate coverage and water of oceanic low-level clouds, Science, 363, eaav0566, doi: 10.1126/science.aav0566, 2019.
Schmale, J., Baccarini, A., Thurnherr, I., Henning, S., Efraim, A., Regayre, L., Bolas, C., Hartmann, M., Welti, A., Lehtipalo, K., Aemisegger, F., Tatzelt, C., Landwehr, S., Modini, R. L., Tummon, F., Johnson, J., Harris, N., Schnaiter, M., Toffoli, A., Derkani, M., Bukowiecki, N., Stratmann, F., Dommen, J., Baltensperger, U., Wernli, H., Rosenfeld, D., Gysel-Beer, M., and Carslaw, K.: Overview of the Antarctic Circumnavigation Expedition: Study of Preindustrial-like Aerosols and Their Climate Effects (ACE-SPACE), B. Am. Meteorol. Soc., doi: 10.1175/bams-d-18-0187.1, 2019.
Scrucca, L., Fop, M., Murphy, T. B., and Raftery, A. E.: mclust 5: Clustering, Classification and Density Estimation Using Gaussian Finite Mixture Models, R. J., 8, 289-317, 2016.
Simmonds, I., Keay, K., and Lim, E.-P.: Synoptic Activity in the Seas around Antarctica, Mon. Weather Rev., 131, 272-288, doi: 10.1175/1520-0493(2003)131<0272:saitsa>2.0.co;2, 2003.
Simpson, R. M. C., Howell, S. G., Blomquist, B. W., Clarke, A. D., and Huebert, B. J.: Dimethyl sulfide: Less important than long-range transport as a source of sulfate to the remote tropical Pacific marine boundary layer, J. Geophys. Res.-Atmos., 119, 9142-9167, doi: doi:10.1002/2014JD021643, 2014.
Stein, A. F., Draxler, R. R., Rolph, G. D., Stunder, B. J. B., Cohen, M. D., and Ngan, F.: NOAA's HYSPLIT Atmospheric Transport and Dispersion Modeling System, B. Am. Meteorol. Soc., 96, 2059-2077, doi: 10.1175/bams-d-14-00110.1, 2015.
Stephens, B. B., Long, M. C., Keeling, R. F., Kort, E. A., Sweeney, C., Apel, E. C., Atlas, E. L., Beaton, S., Bent, J. D., Blake, N. J., Bresch, J. F., Casey, J., Daube, B. C., Diao, M., Diaz, E., Dierssen, H., Donets, V., Gao, B.-C., Gierach, M., Green, R., Haag, J., Hayman, M., Hills, A. J., Hoecker-Martínez, M. S., Honomichl, S. B., Hornbrook, R. S., Jensen, J. B., Li, R.-R., McCubbin, I., McKain, K., Morgan, E. J.,

Nolte, S., Powers, J. G., Rainwater, B., Randolph, K., Reeves, M., Schauffler, S. M., Smith, K., Smith, M., Stith, J., Stossmeister, G., Toohey, D. W., and Watt, A. S.: The O2/N2 Ratio and CO2 Airborne Southern Ocean Study, B. Am. Meteorol. Soc., 99, 381-402, doi: 10.1175/bams-d-16-0206.1, 2018.

Vignati, E., Facchini, M. C., Rinaldi, M., Scannell, C., Ceburnis, D., Sciare, J., Kanakidou, M., Myriokefalitakis, S., Dentener, F., and O'Dowd, C. D.: Global scale emission and distribution of sea-spray aerosol: Sea-salt and organic enrichment, Atmos. Environ., 44, 670-677, doi: 10.1016/j.atmosenv.2009.11.013, 2010.

Weigum, N., Schutgens, N., and Stier, P.: Effect of aerosol subgrid variability on aerosol optical depth and cloud condensation nuclei: implications for global aerosol modelling, Atmos. Chem. Phys., 16, 13619-13639, doi: 10.5194/acp-16-13619-2016, 2016.

Williams, K. D., Bodas-Salcedo, A., Déqué, M., Fermepin, S., Medeiros, B., Watanabe, M., Jakob, C., Klein, S. A., Senior, C. A., and Williamson, D. L.: The Transpose-AMIP II Experiment and Its Application to the Understanding of Southern Ocean Cloud Biases in Climate Models, J. Climate, 26, 3258-3274, doi: 10.1175/jcli-d-12-00429.1, 2013.

Williamson, C. J., Kupc, A., Axisa, D., Bilsback, K. R., Bui, T., Campuzano-Jost, P., Dollner, M., Froyd, K. D., Hodshire, A. L., Jimenez, J. L., Kodros, J. K., Luo, G., Murphy, D. M., Nault, B. A., Ray, E. A., Weinzierl, B., Wilson, J. C., Yu, F., Yu, P., Pierce, J. R., and Brock, C. A.: A large source of cloud condensation nuclei from new particle formation in the tropics, Nature, 574, 399-403, doi: 10.1038/s41586-019-1638-9, 2019.

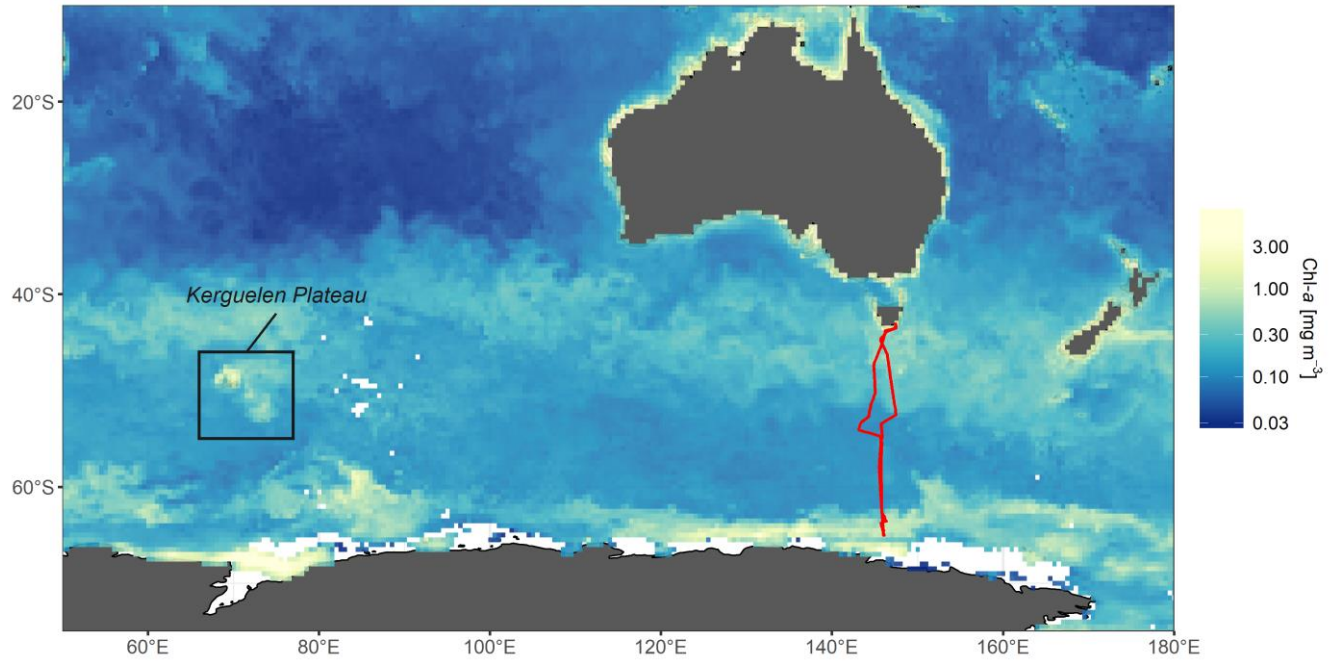

Figure 1: Voyage track (red line) of the RV Investigator during the CWT voyage. The colour scale represents the mean chlorophyll-a concentrations for February 2015, derived from MODIS satellite images. A logarithmic scale has been used and has been limited to the range 0.03–7 mg m^{-3} to enhance visual detail. White regions represent unavailable data due to sea ice or persistent cloud cover, and a region of high marine biological activity has been marked in the vicinity of the Kerguelen Plateau.

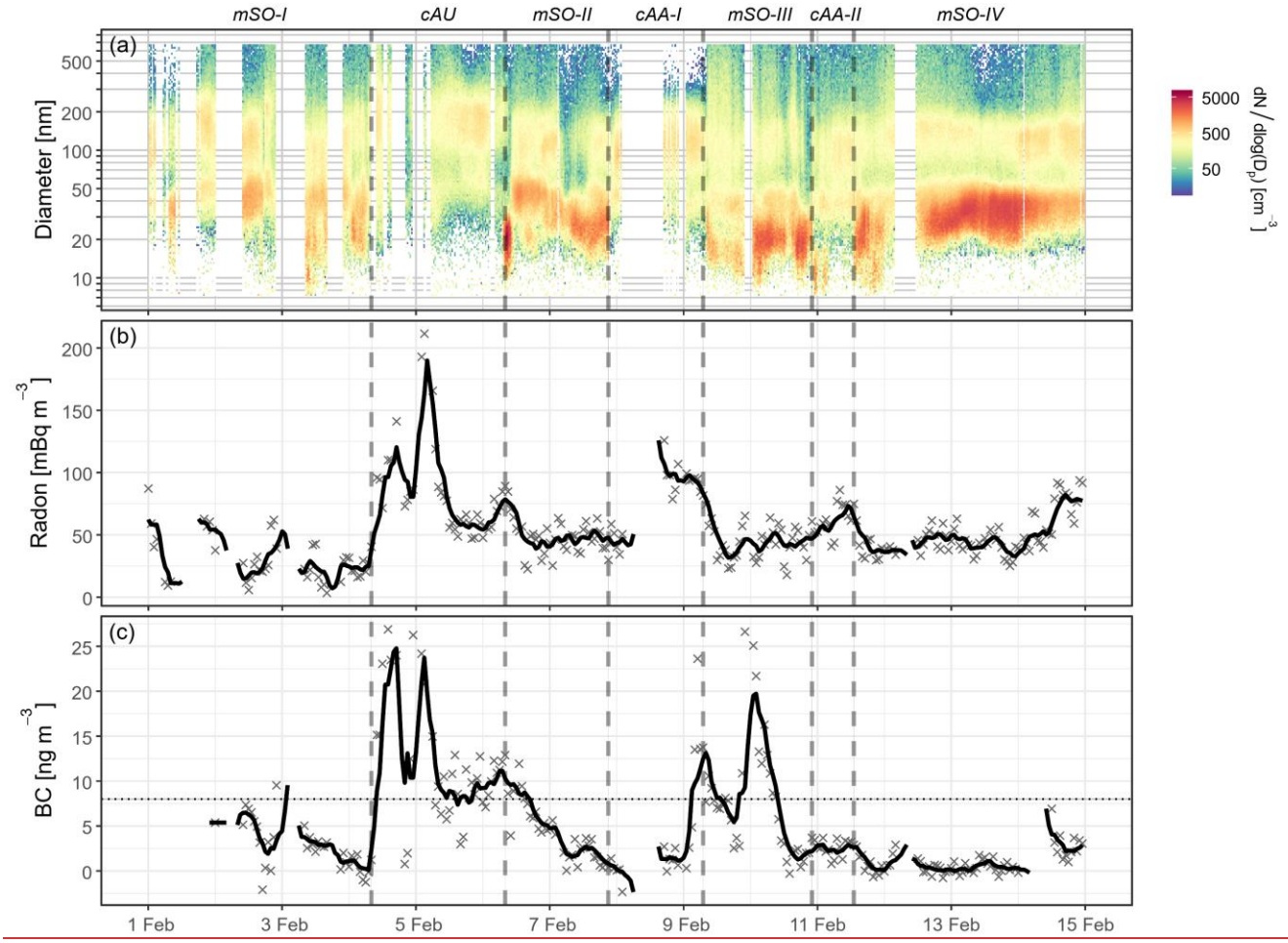

Figure 2. Time series of (a) aerosol size distributions, (b) atmospheric radon concentrations and (c) BC concentrations throughout the Cold Water Trial voyage. Periods influenced by different air masses are labelled and delimited by dotted lines. Blank regions represent periods of instrument maintenance or contamination from ship emissions which have been excluded from analysis. The smoothed black lines in (b) and (c) represent rolling six-hour averages to assist in identification of temporal trends. Periods influenced by ship emissions have been removed from the BC concentrations and the dotted horizontal line gives the BC detection limit of 8 ng m^{-3}.

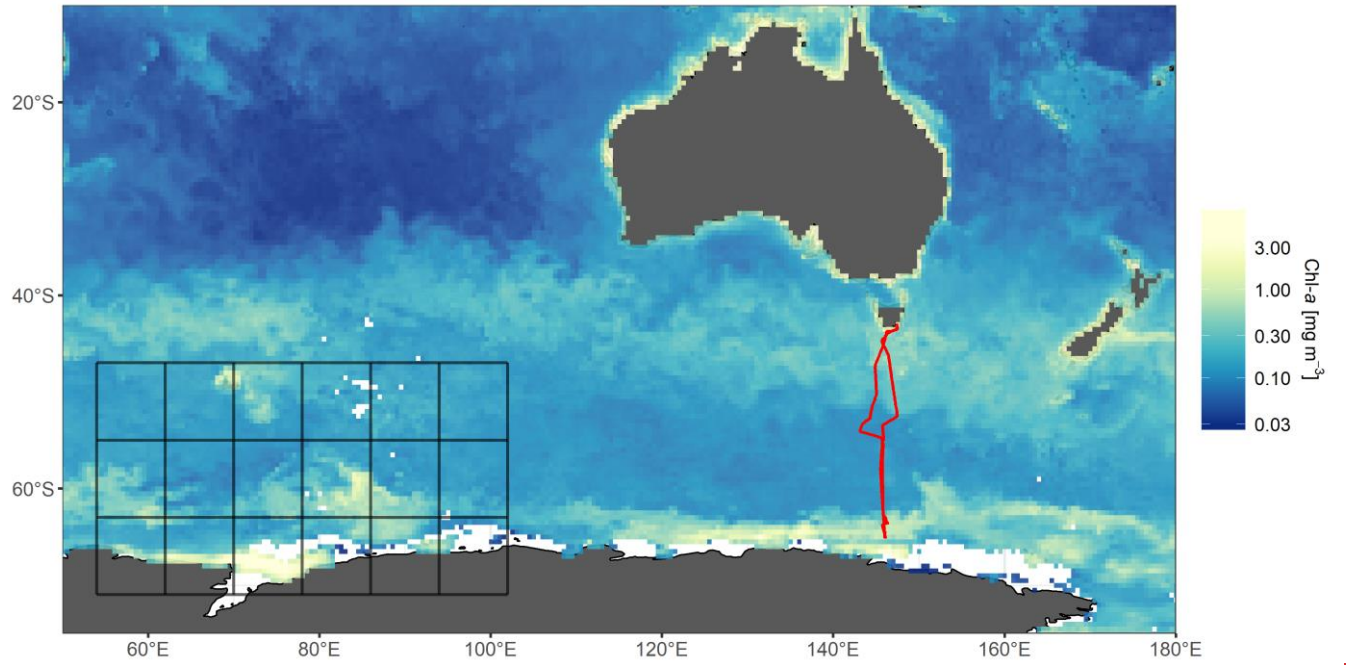

~~**Figure 1: Mean chlorophyll-a concentrations for February 2015, derived from MODIS satellite images. A logarithmic colour scale has been used and has been limited to the range 0.03–7 mg m^{-3} to enhance visual detail. White regions represent unavailable data due to sea ice or persistent cloud cover. The black grid represents the cell boundaries used to rasterize Chl-a concentrations in the Kerguelen-Antaretic productive region. The ship's voyage track is represented in red.**~~

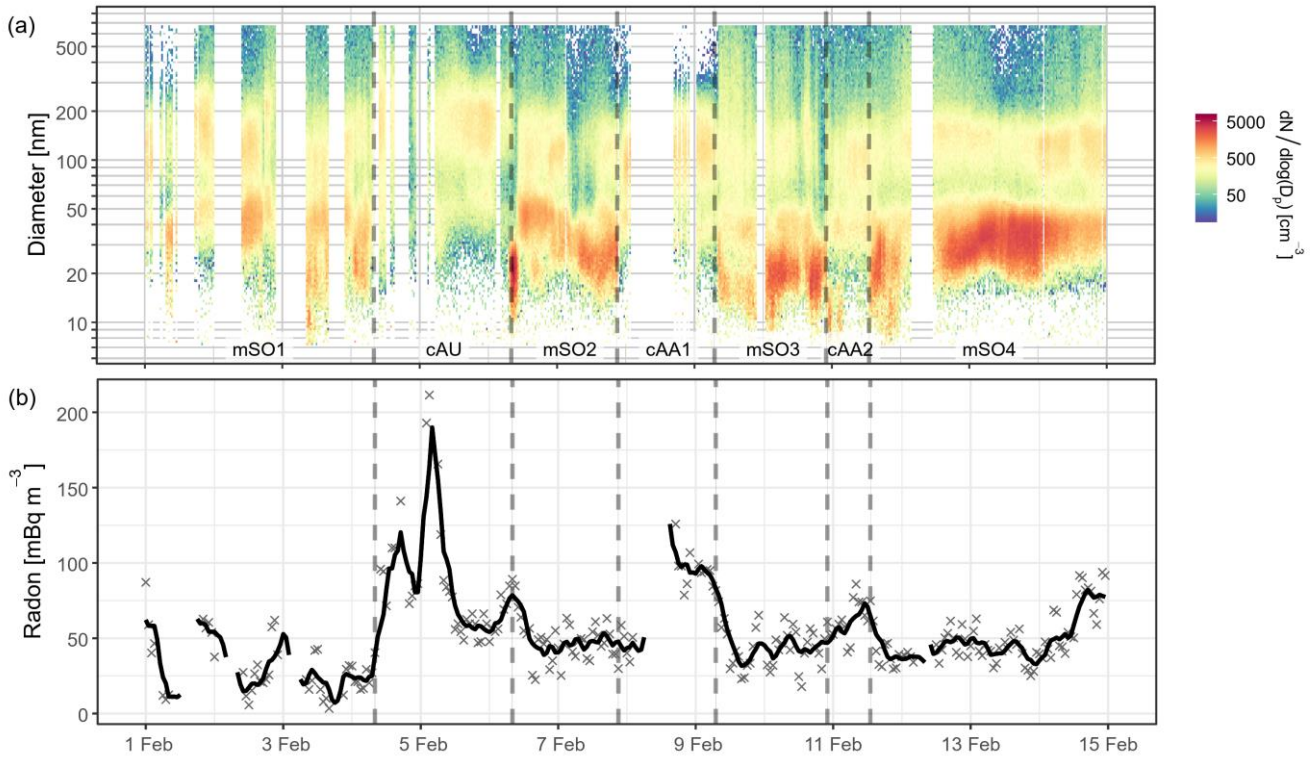

~~**Figure 2. Time series of (a) aerosol size distributions and (b) atmospheric radon concentrations throughout the Cold Water Trial voyage. Periods influenced by different air masses are labelled and delimited by dotted lines. Blank regions represent periods of instrument maintenance or contamination from ship emissions which have been excluded from analysis. The smoothed black line represents a rolling six-hour average of the radon concentrations to assist in identification of temporal trends.**~~

Table 1: Mean physical properties observed for the three air mass classifications, presented as the mean for each air mass ± the standard deviation.

Air mass	*cAA*	*cAU*	*mSO*
Number concentrations			
N_{10} (cm^{-3})	310 ± 37	220 ± 70	540 ± 200
$CCN_{0.5\%}$ (cm^{-3})	210 ± 45	180 ± 65	190 ± 65
$CCN_{0.5\%}$ activation ratio	0.68 ± 0.17	0.79 ± 0.11	0.35 ± 0.18
Size distributions			
Aitken number fraction	0.40 ± 0.16	0.40 ± 0.07	0.71 ± 0.14
Aitken mean diameter (nm)	31 ± 9	43 ± 11	30 ± 6
Accumulation mean diameter (nm)	115 ± 14	191 ± 18	137 ± 24
Hoppel minimum diameter (nm)	57 ± 7	76 ± 7	69 ± 8
Hygroscopicity			
κ_{D40}	0.41 ± 0.10	0.38 ± 0.09	0.38 ± 0.08
κ_{D100}	0.39 ± 0.08	0.37 ± 0.04	0.44 ± 0.08
κ_{D150}	0.51 ± 0.12	0.46 ± 0.07	0.52 ± 0.12
Volatility			
VFR_{D40}	0.97 ± 0.09	0.89 ± 0.03	0.89 ± 0.11
VFR_{D100}	0.94 ± 0.07	0.85 ± 0.03	0.90 ± 0.07
VFR_{D150}	0.94 ± 0.08	0.92 ± 0.02	0.91 ± 0.07
Composition			
Org ($\mu g\ m^{-3}$)	BDL[1]	0.08 ± 0.05	BDL
SO_4 ($\mu g\ m^{-3}$)	0.12 ± 0.03	0.18 ± 0.08	0.12 ± 0.06
SSA ($\mu g\ m^{-3}$)	0.08 ± 0.07	0.12 ± 0.10	0.21 ± 0.18
Continental / anthropogenic influences			
Radon ($mBq\ m^{-3}$)	73 ± 22	83 ± 38	43 ± 17
BC ($ng\ m^{-3}$)	4 ± 5	12 ± 6	5 ± 6

[1] *Below detection limit*

Table 1: Physical properties observed for the three air mass classifications, including continental Antarctic (*cAA*), continental Australian (*cAU*) and maritime Southern Ocean (*mSO*). The values represent the median for each air mass, with the interquartile range provided in parentheses.

Air mass	*cAA*	*cAU*	*mSO*
Number concentrations			
N_{10} (cm^{-3})	308 (291–329)	239 (166–259)	492 (408–664)
$CCN_{0.5\%}$ (cm^{-3})	224 (198–252)	200 (127–225)	188 (145–228)
$CCN_{0.5\%}$ activation ratio	0.71 (0.62–0.80)	0.80 (0.72–0.89)	0.40 (0.28–0.55)
Size distributions			
Nucleation concentration (cm^{-3})	32 (15–75)	13 (10–15)	240 (120–490)
Aitken concentration (cm^{-3})	74 (65–81)	65 (43–77)	190 (110–280)
Accumulation concentration (cm^{-3})	180 (150–210)	170 (130–180)	140 (100–170)
Nucleation peak diameter (nm)	13 (11–17)	23 (22–25)	21 (19–27)
Aitken peak diameter (nm)	37 (36–39)	51 (45–57)	37 (34–42)
Accumulation peak diameter (nm)	102 (96–115)	172 (169–181)	121 (111–129)
Nucleation mode spread	1.36 (1.28–1.50)	1.33 (1.10–1.45)	1.33 (1.25–1.45)
Aitken mode spread	1.28 (1.24–1.34)	1.45 (1.34–1.57)	1.3 (1.24–1.35)
Accumulation mode spread	1.58 (1.53–1.67)	1.62 (1.53–1.70)	1.59 (1.49–1.70)
Composition			
Org ($ng\ m^{-3}$)	< 50*	80 (50–110)	< 50*
SO_4 ($ng\ m^{-3}$)	130 (100–140)	180 (120–250)	100 (70–130)
SSA ($ng\ m^{-3}$)	60 (20–120)	90 (40–170)	140 (80–30)
Continental / anthropogenic influences			
Radon ($mBq\ m^{-3}$)	74 (56–94)	73 (60–89)	42 (31–54)
BC ($ng\ m^{-3}$)	< 8*	10 (8–15)	< 8*

* *Below detection limit*

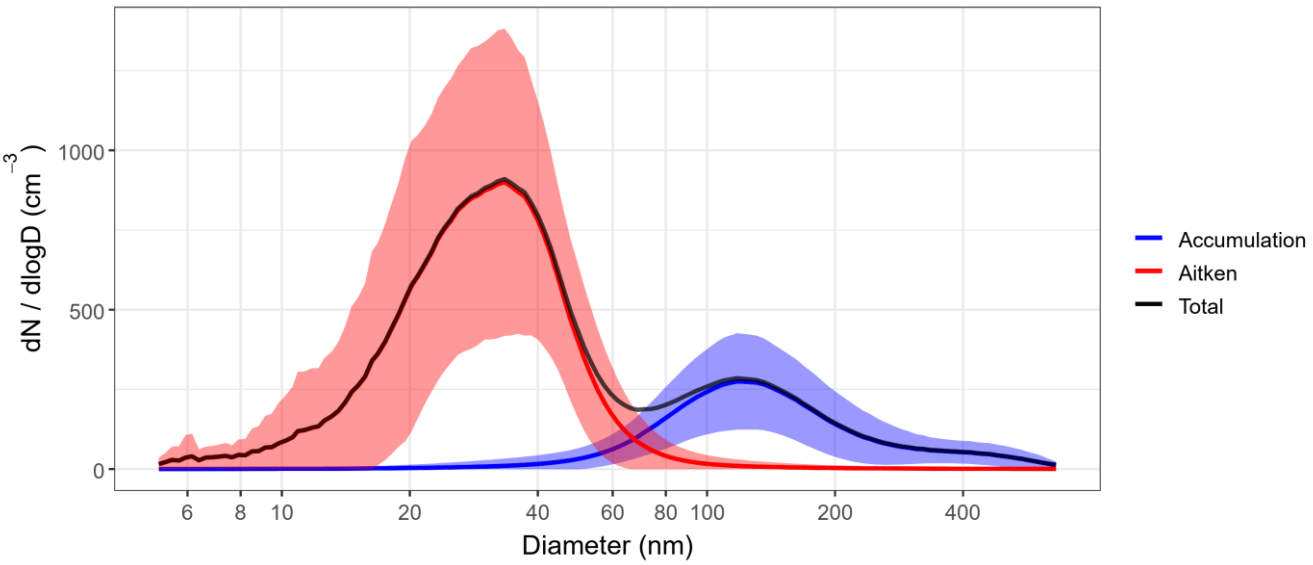

~~**Figure 3: Mean number size distribution for sub-micron aerosol during periods of *mSO* air masses. The coloured lines are fitted log-normal distributions representing contributions from Aitken and accumulation mode aerosol to the observed (black) total size distribution. The shaded regions give the standard deviations of the fitted modes throughout the *mSO* sampling periods.**~~

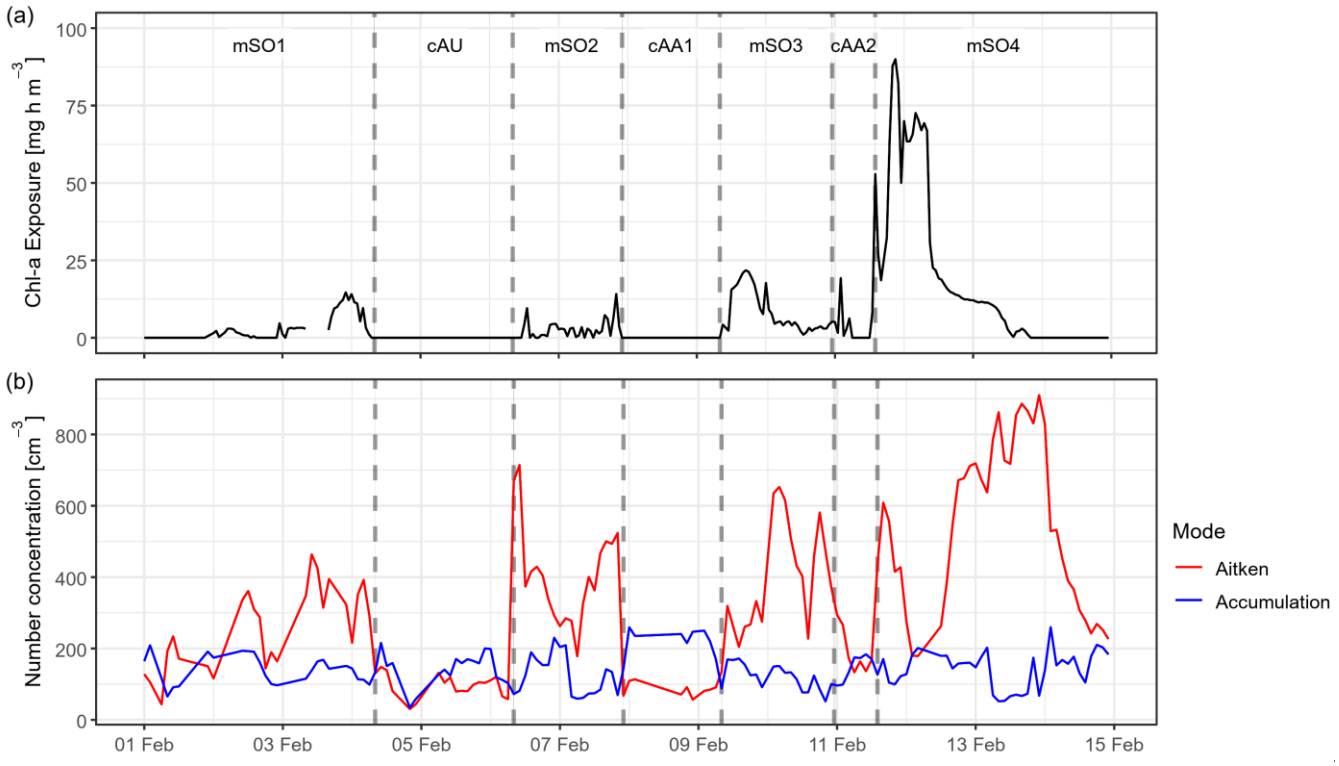

~~**Figure 4: (a) Summed Chl-a concentration as a proxy for total flux of biogenic aerosol precursors received by each air mass during time spent within the MBL over the productive Kerguelen Antarctic region. (b) Aerosol number concentrations in the Aitken and accumulation modes, as derived from the fitted size distributions. Periods influenced by different air masses are labelled and delimited by dotted lines.**~~

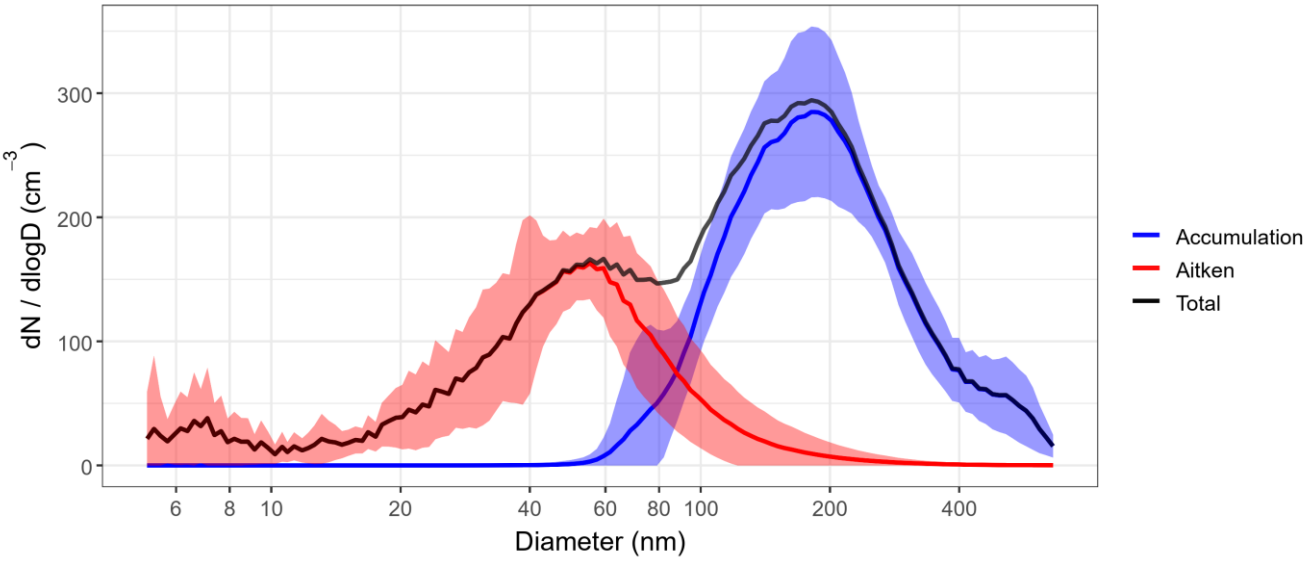

~~**Figure 5: Mean number size distribution for sub-micron aerosol during a period likely influenced by continental and coastal Australian air masses. The coloured lines are fitted log-normal distributions representing contributions from Aitken and accumulation mode aerosol to the observed (black) total size distribution. The shaded regions give the standard deviations of the fitted modes throughout the *cAU* sampling periods.**~~

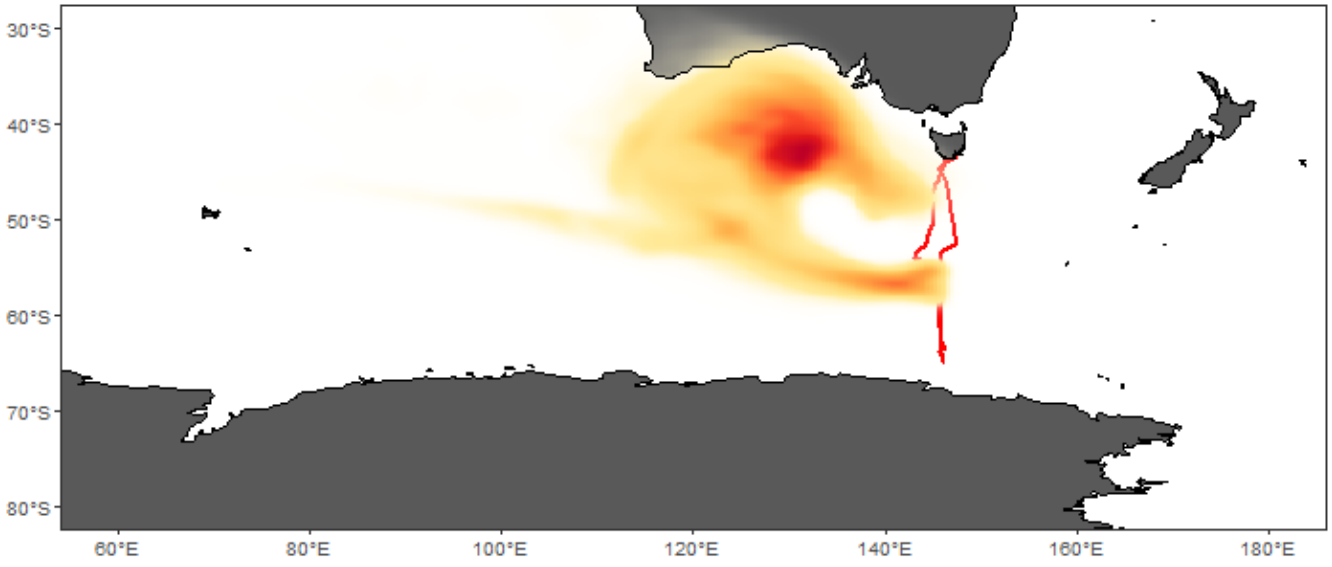

~~Figure 6: Probability distribution of air mass coordinates throughout all back trajectory ensembles from the *cAU* sampling period. The colour scale reflects the proportion of trajectories which passed through each location, with the highest density of~~

~~trajectories found in the dark red region, which coincided with the approximate centre of a high-pressure system. The ship's voyage track is represented in red and the ship was located at a mean latitude of 56° S during this period.~~

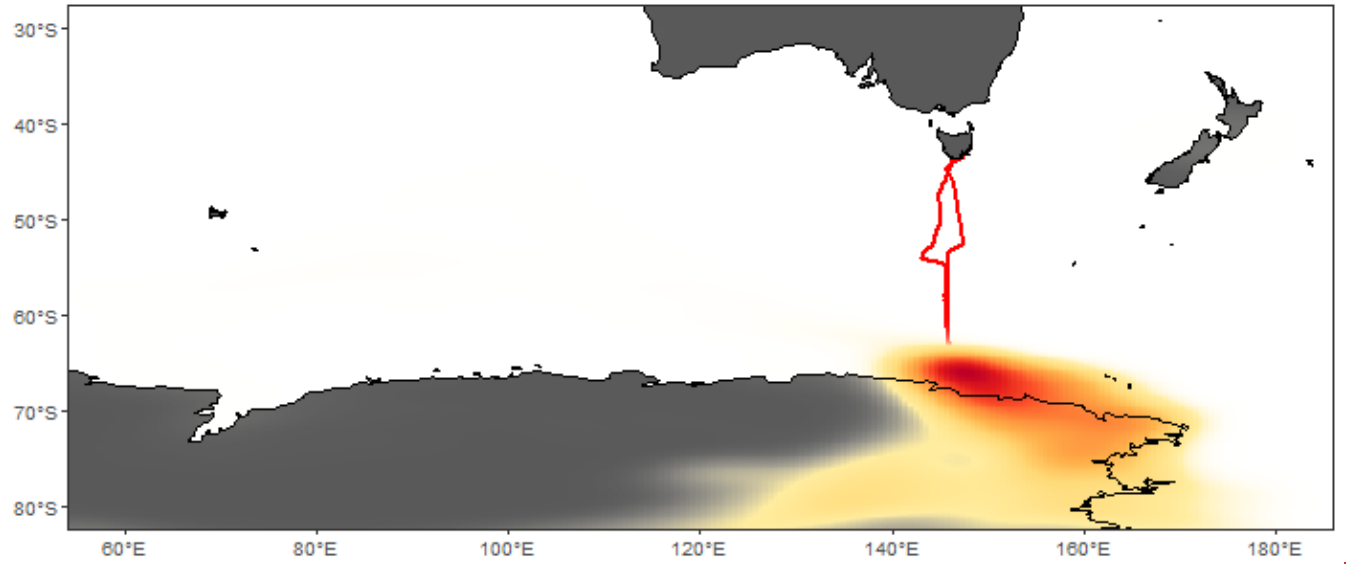

~~Figure 7: Probability distribution of air mass coordinates throughout all back trajectory ensembles from the *cAA1* sampling period. The colour scale reflects the proportion of trajectories which passed through each location, with the highest density of trajectories found in the dark red region. The ship's voyage track is represented in red and the ship was located at a mean latitude of 64.5° S during this period.~~

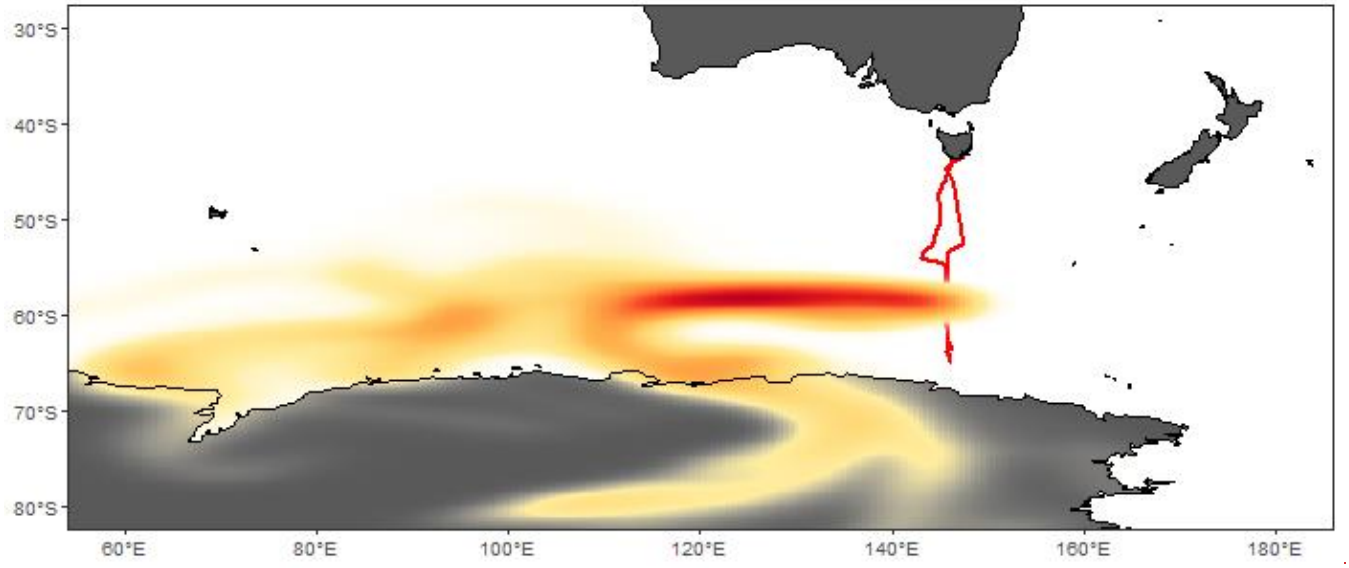

~~Figure 8: Probability distribution of air mass coordinates throughout all back trajectory ensembles from the *cAA2* sampling period. The colour scale reflects the proportion of trajectories which passed through each location, with the highest density of~~

~~trajectories found in the dark red region. The ship's voyage track is represented in red and the ship was located at a mean latitude of 59° S during this period.~~

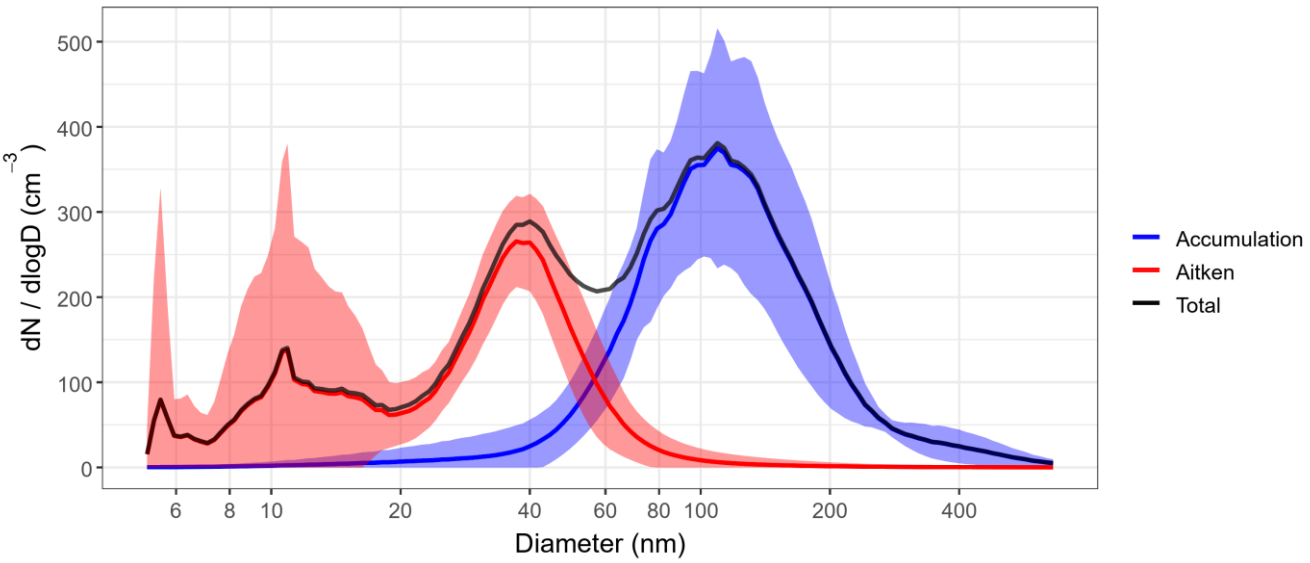

~~Figure 9: Mean number size distribution for sub-micron aerosol during two sampling periods influenced by continental Antarctic air masses. The coloured lines are fitted log-normal distributions representing contributions from Aitken and accumulation mode aerosol to the observed (black) total size distribution. The shaded regions give the standard deviations of the fitted modes throughout the *cAA* sampling periods.~~

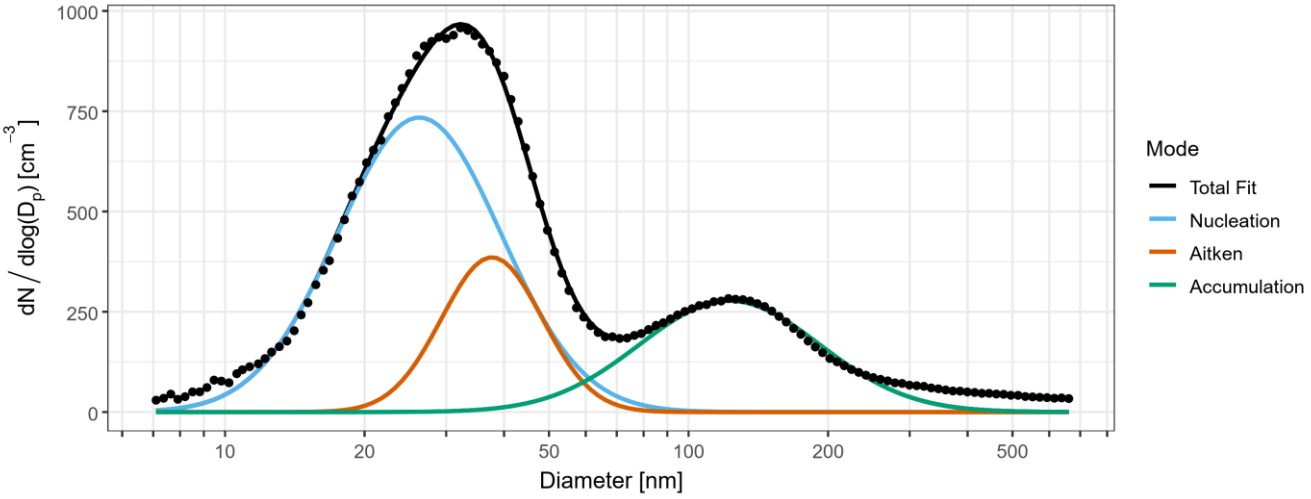

Figure 3: Mean number size distribution for sub-micron aerosol during periods of *mSO* air masses. The coloured lines are fitted log-normal distributions representing contributions from nucleation (blue), Aitken (brown) and accumulation (green) mode aerosol to the observed total size distribution (black points).

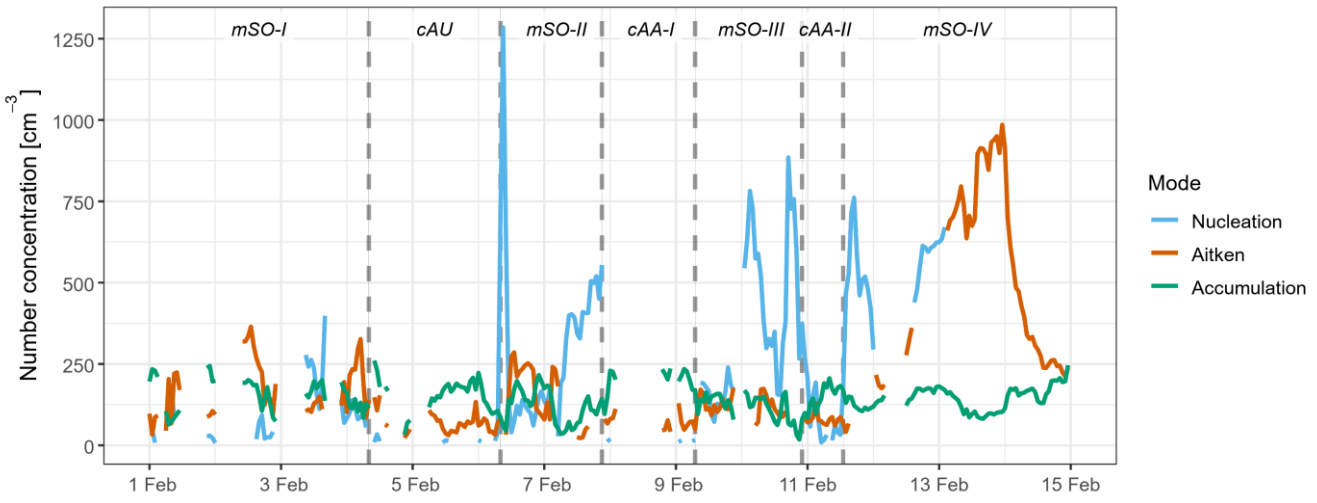

Figure 4: Aerosol number concentrations in the nucleation (blue), Aitken (brown) and accumulation (green) modes, as derived from the fitted size distributions. Periods influenced by different air masses are labelled and delimited by dotted lines. Blank regions represent missing data due to contamination from ship emissions or instrument maintenance.

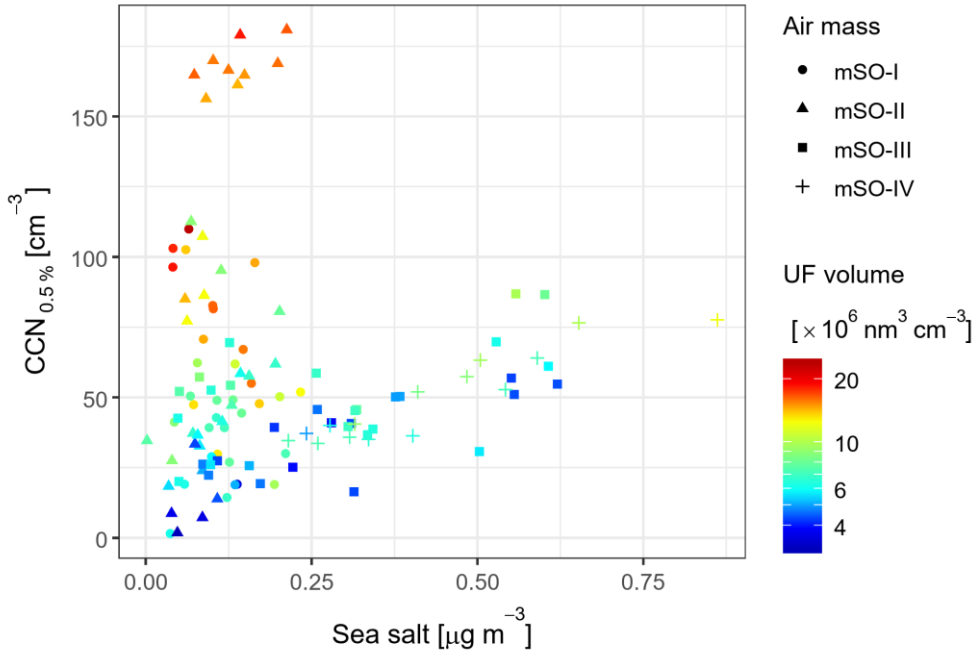

Figure 5: Correlations between non-accumulation mode $CCN_{0.5\%}$ and sea salt mass concentrations derived from ACSM measurements. The point shapes represent the four periods affected by marine air masses, while the colour scale represents the corresponding volume concentrations of ultrafine aerosol. The Pearson's correlation coefficients (and p-values) were 0.169 (0.30), 0.495 (3.4×10^{-3}), 0.516 (1.5×10^{-3}) and 0.929 (5.6×10^{-7}) for each air mass in chronological order.

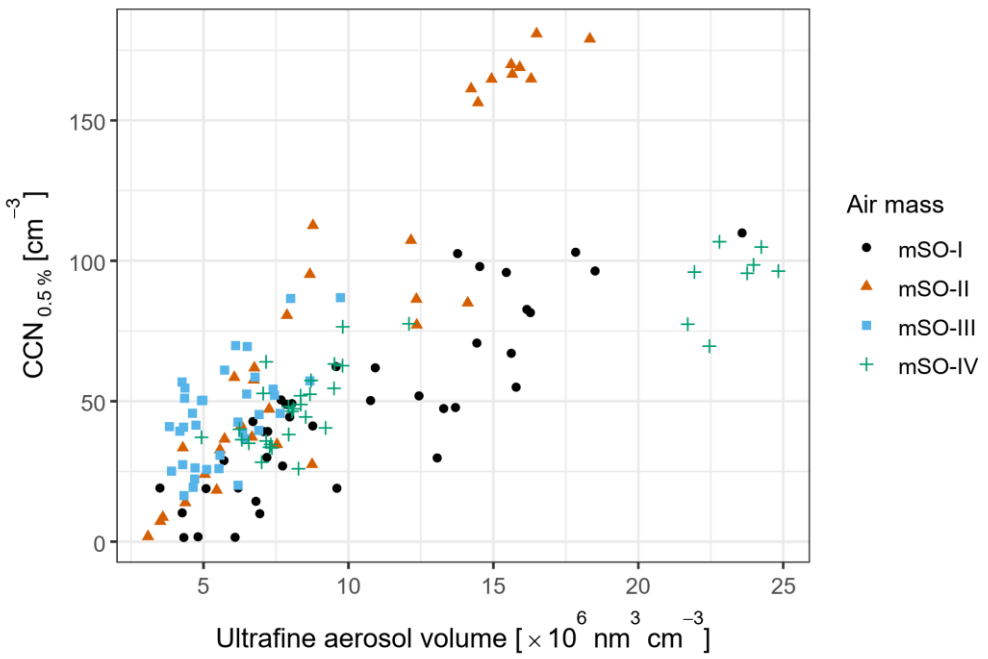

Figure 6: Correlations between non-accumulation mode $CCN_{0.5\%}$ and total ultrafine aerosol volume concentration. The point shapes and colours represent the four periods affected by marine air masses. The Pearson's correlation coefficients (and p-values) were 0.888 (4.3×10^{-15}), 0.942 (3.2×10^{-16}), 0.580 (2.1×10^{-4}), and 0.888 (1.1×10^{-12}) for each air mass in chronological order.

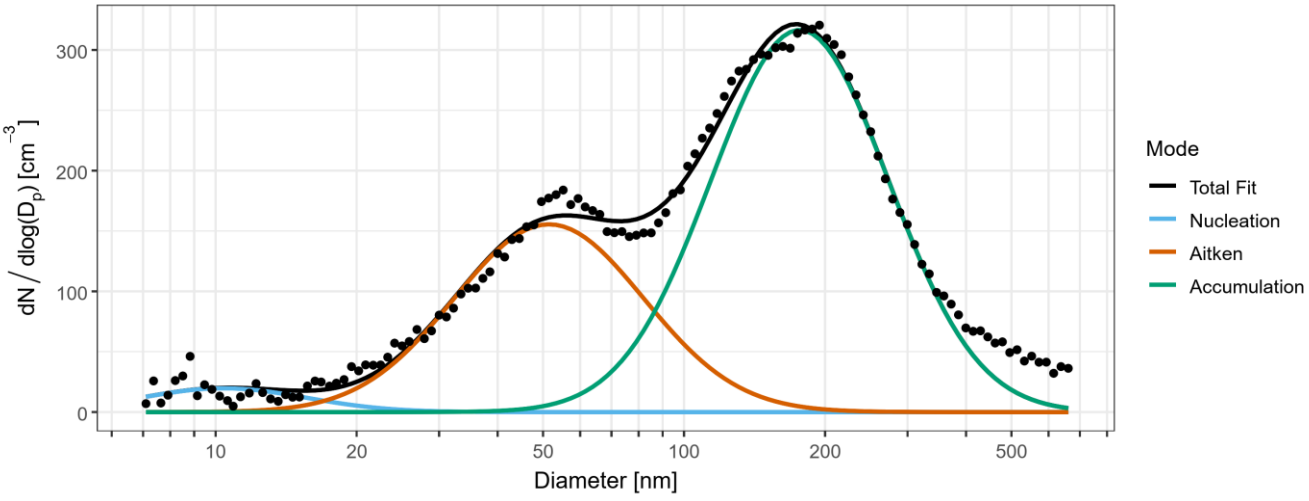

Figure 7: Mean number size distribution for sub-micron aerosol during a period likely influenced by continental and coastal Australian air masses. The coloured lines are fitted log-normal distributions representing contributions from nucleation (blue), Aitken (brown) and accumulation (green) mode aerosol to the observed total size distribution (black points).

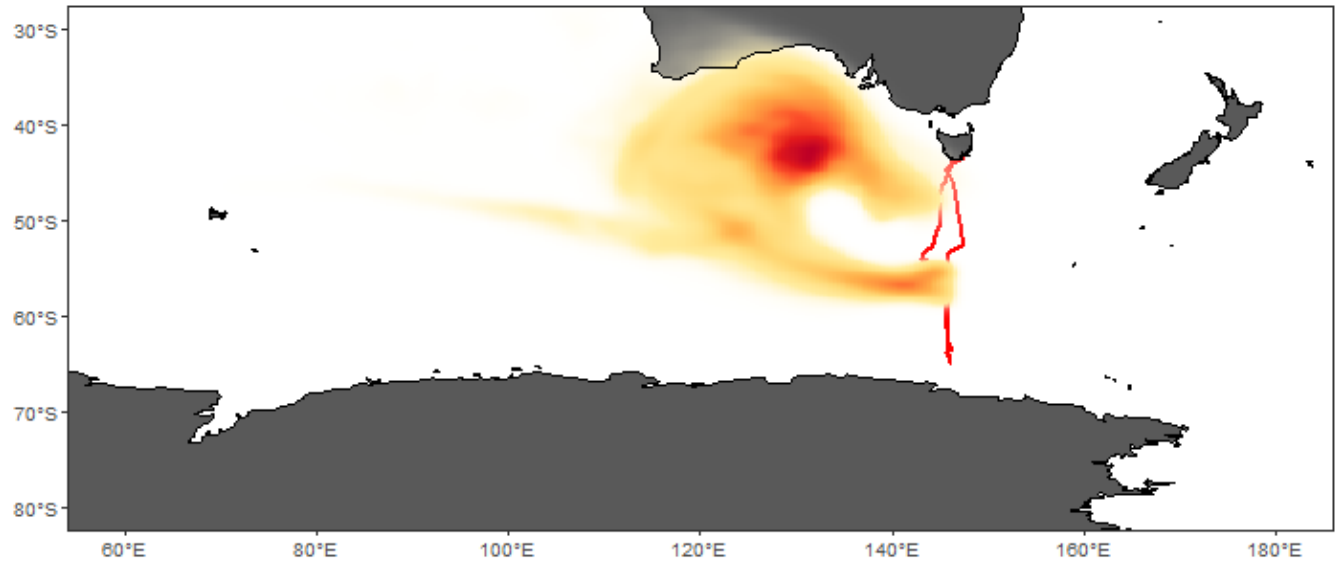

Figure 8: Probability distribution of air mass coordinates throughout all back trajectory ensembles from the *cAU* sampling period. The colour scale reflects the proportion of trajectories which passed through each location, with the highest density of trajectories found in the dark red region, which coincided with the approximate centre of a high-pressure system. The ship's voyage track is represented in red and the ship was located at a mean latitude of 56° S during this period.

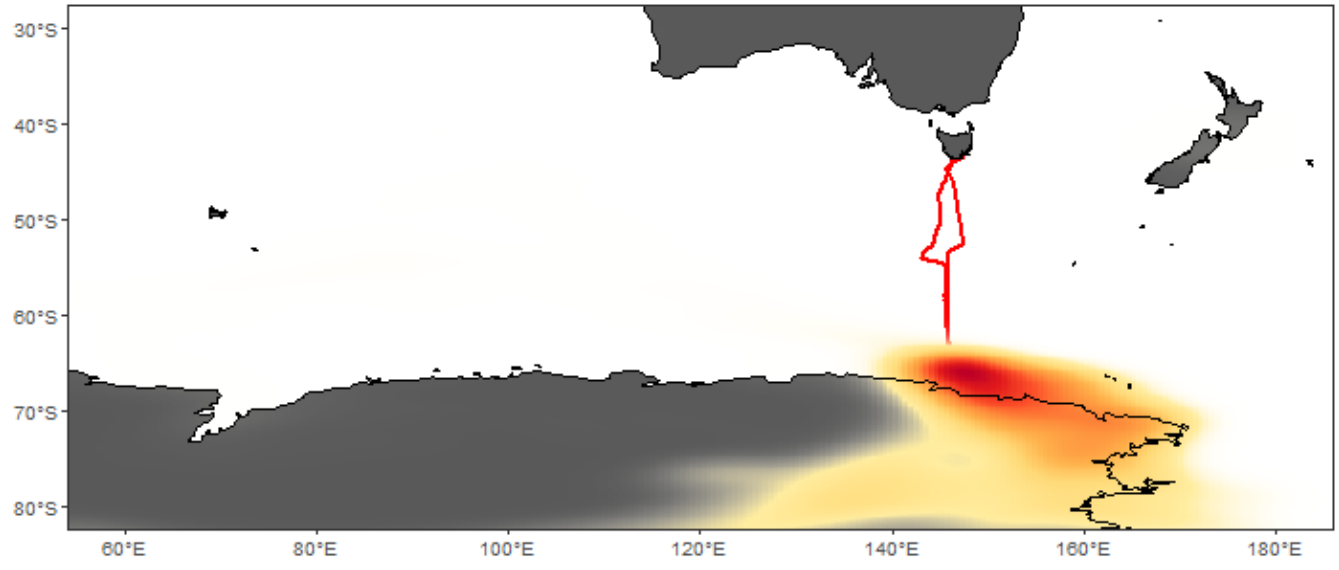

Figure 9: Probability distribution of air mass coordinates throughout all back trajectory ensembles from the *cAA-I* sampling period. The colour scale reflects the proportion of trajectories which passed through each location, with the highest density of trajectories found in the dark red region. The ship's voyage track is represented in red and the ship was located at a mean latitude of 64.5° S during this period.

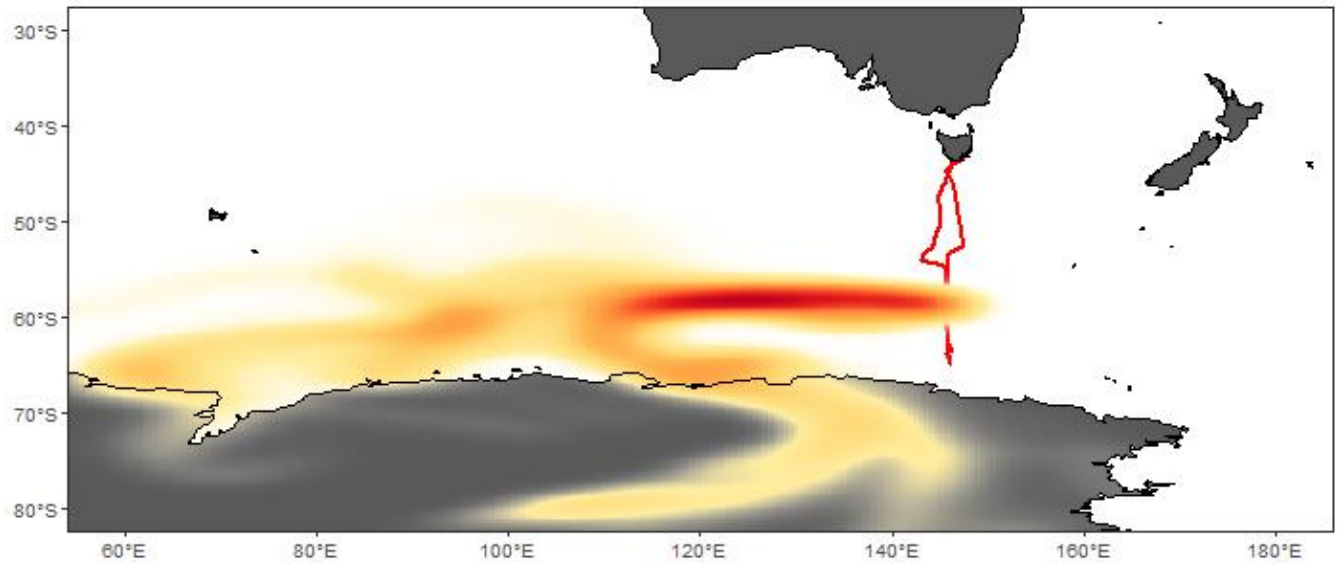

Figure 10: Probability distribution of air mass coordinates throughout all back trajectory ensembles from the *cAA-II* sampling period. The colour scale reflects the proportion of trajectories which passed through each location, with the highest density of trajectories found in the dark red region. The ship's voyage track is represented in red and the ship was located at a mean latitude of 59° S during this period.

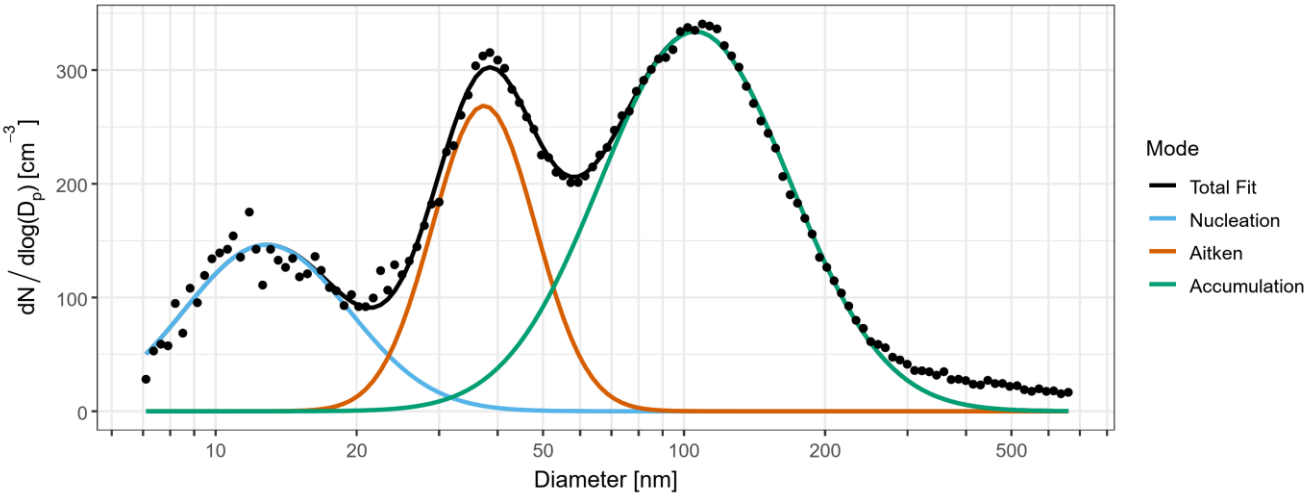

Figure 11: Mean number size distribution for sub-micron aerosol during two sampling periods influenced by continental Antarctic air masses. The coloured lines are fitted log-normal distributions representing contributions from nucleation (blue), Aitken (brown) and accumulation (green) mode aerosol to the observed total size distribution (black points).